



THE UNIVERSITY *of* EDINBURGH

## Edinburgh Research Explorer

# Infectiondriven activation of transglutaminase 2 boosts glucose uptake and hexosamine biosynthesis in epithelial cells

### Citation for published version:

Maffei, B, Laverrière, M, Wu, Y, Triboulet, S, Perrinet, S, Duchateau, M, Matondo, M, Hollis, RL, Gourley, C, Rupp, J, Keillor, JW & Subtil, A 2020, 'Infectiondriven activation of transglutaminase 2 boosts glucose uptake and hexosamine biosynthesis in epithelial cells', *The EMBO journal*, vol. 39, no. 8.  
<https://doi.org/10.15252/embj.2019102166>

### Digital Object Identifier (DOI):

[10.15252/embj.2019102166](https://doi.org/10.15252/embj.2019102166)

### Link:

[Link to publication record in Edinburgh Research Explorer](#)

### Document Version:

Peer reviewed version

### Published In:

The EMBO journal

### Publisher Rights Statement:

This is a pre-copyedited, author-produced version of an article accepted for publication in The EMBO Journal following peer review. The version of record "Infectiondriven activation of transglutaminase 2 boosts glucose uptake and hexosamine biosynthesis in epithelial cells" is available online at <https://doi.org/10.15252/embj.2019102166>

### General rights

Copyright for the publications made accessible via the Edinburgh Research Explorer is retained by the author(s) and / or other copyright owners and it is a condition of accessing these publications that users recognise and abide by the legal requirements associated with these rights.

### Take down policy

The University of Edinburgh has made every reasonable effort to ensure that Edinburgh Research Explorer content complies with UK legislation. If you believe that the public display of this file breaches copyright please contact [openaccess@ed.ac.uk](mailto:openaccess@ed.ac.uk) providing details, and we will remove access to the work immediately and investigate your claim.



**Infection-driven activation of transglutaminase 2**  
**boosts glucose uptake and hexosamine biosynthesis**

Benoit Maffei<sup>1,2</sup>, Marc Laverrière<sup>1</sup>, Yongzheng Wu<sup>1</sup>, Sébastien Triboulet<sup>1</sup>, Stéphanie Perrinet<sup>1</sup>, Magalie Duchateau<sup>3</sup>, Mariette Matondo<sup>3</sup>, Robert L. Hollis<sup>4</sup>, Charlie Gourley<sup>4</sup>, Jan Rupp<sup>5</sup>, Jeffrey W. Keillor<sup>6</sup> and Agathe Subtil<sup>1\*</sup>

<sup>1</sup> Unité de Biologie cellulaire de l'infection microbienne, Institut Pasteur, CNRS UMR3691, 75015 Paris, France

<sup>2</sup> Sorbonne Université, Collège Doctoral, F-75005 Paris, France

<sup>3</sup> Plateforme Protéomique, Unité de Spectrométrie de Masse pour la Biologie, USR 2000 CNRS, Institut Pasteur, Paris, France

<sup>4</sup> Nicola Murray Centre for Ovarian Cancer Research, Cancer Research UK Edinburgh Centre, MRC IGMM, University of Edinburgh, Edinburgh, UK

<sup>5</sup> Department of Infectious Diseases and Microbiology, University of Lübeck, Lübeck, Germany

<sup>6</sup> Department of Chemistry and Biomolecular Sciences, University of Ottawa, Canada

\* Corresponding author: Unité de Biologie cellulaire de l'infection microbienne  
25 rue du Dr Roux, 75015 Paris, France  
Tel: +33 1 40 61 30 49  
Fax: + 33 1 40 61 32 38  
E-mail: [asubtil@pasteur.fr](mailto:asubtil@pasteur.fr)

29 ABSTRACT

30  
31  
32 Transglutaminase 2 (TG2) is a ubiquitous enzyme with transamidating activity. We  
33 report here that the expression and activity of TG2 are enhanced in cells infected with the  
34 obligate intracellular bacteria *Chlamydia trachomatis*. Genetic or pharmacological inhibition  
35 of TG2 activity impair bacterial development. We show that TG2 increases glucose import by  
36 up-regulating the transcription of the glucose transporter genes *GLUT-1* and *GLUT-3*.  
37 Furthermore, TG2 activation drives one specific glucose-dependent pathway in the host, i.e.  
38 hexosamine biosynthesis. Mechanistically, we identify the glucosamine:fructose-6-phosphate  
39 amidotransferase (GFPT) among the substrates of TG2. GFPT modification by TG2 increases  
40 its enzymatic activity, resulting in higher levels of UDP-N-acetylglucosamine biosynthesis. As  
41 a consequence, TG2 activation results in increased protein O-GlcNAcylation. The correlation  
42 between TG2 transamidating activity and O-GlcNAcylation is disrupted in infected cells  
43 because host hexosamine biosynthesis is being exploited by the bacteria, in particular to assist  
44 their division. In conclusion, our work establishes TG2 as a key player in controlling glucose-  
45 derived metabolic pathways in mammalian cells, themselves hijacked by *C. trachomatis* to  
46 sustain their own metabolic needs.

47  
48  
49 KEYWORDS: Chlamydia / GFPT / Hexosamine biosynthesis / O-GlcNAcylation /  
50 Transglutaminase 2

## INTRODUCTION

The enzyme transglutaminase 2 (TG2) is an extremely versatile protein exhibiting transamidase, protein disulfide isomerase and guanine and adenine nucleotide binding and hydrolyzing activities (Gundemir, Colak et al., 2012). Also designated as “tissue transglutaminase”, it is ubiquitously expressed in the cytoplasm and at the cell surface in association with the extracellular matrix (Eckert, Kaartinen et al., 2014). The transamidase activity is the best described activity, and it is regulated by  $\text{Ca}^{2+}$  (Folk, Mullooly et al., 1967). It results in the formation of cross-links between proteins, or of post-translational modification of a protein substrate through incorporation of a small primary amine, or deamidation of a glutamine into a glutamate. Under steady-state conditions, TG2 exists in a compact, inactive conformation. Increase in intracellular  $\text{Ca}^{2+}$  concentration (upon stress, cell activation, etc) causes a conformational change, and the enzyme becomes catalytically active as a transamidase. Studies of genetically engineered mouse models and/or inherited disorders have implicated TG2 in several pathological conditions (Iismaa, Mearns et al., 2009). In particular, increased TG2 expression and transamidation activity is a common feature of many inflammatory diseases and events (Eckert et al., 2014). Possibly linked to its increased expression in inflammatory processes, several lines of evidence suggest the involvement of TG2 during cancer development (Huang, Xu et al., 2015).

Surprisingly, while the association between TG2 activity and inflammatory situations has been studied in several normal and pathological situations (Di Sabatino, Vanoli et al., 2012, Huang et al., 2015, Ientile, Curro et al., 2015, Iismaa et al., 2009, Liu, Kellems et al., 2017), the implication of this enzyme in a very classical inflammatory process, e.g. the defense response of a tissue to the invasion by a microorganism, has remained very poorly investigated. *Chlamydia trachomatis* is the most common sexually transmitted bacterial pathogen, and it develops inside a vacuole in a human host cell, typically an epithelial cell of the genital tract (reviewed in (AbdelRahman & Belland, 2005)). This obligate intracellular bacterium depends on the host to supply several essential metabolites, and in particular glucose (Gehre, Gorgette et al., 2016, Stephens, Kalman et al., 1998). Epithelial cells respond to the infection with the secretion of proinflammatory cytokines such as interleukin-6 (IL-6) and IL-8 (Rasmussen, Eckmann et al., 1997). The inflammatory response is exacerbated upon reinfection, ultimately leading to tissue damage such as hydrosalpinx and fibrosis (Brunham & Rey-Ladino, 2005). In this work, we show that TG2 becomes activated during the infection of epithelial cells with *C. trachomatis*, and is required for optimal bacterial growth. The investigation of the consequence of TG2 activation on host metabolism and the identification of targets of TG2 transamidase activity during infection uncovered the control exerted by this enzyme on glucose import and on the hexosamine biosynthesis pathway, two metabolic features that are exploited by *C. trachomatis*.

## RESULTS

### **TG2 is highly expressed and becomes active during *C. trachomatis* infection**

A widely-used technique to probe TG2 activation is to measure the incorporation of biotin pentylamine (BP) into proteins. When present in excess, this membrane permeable primary amine out-competes other substrates for the transamidase reaction catalyzed by TG2 and becomes covalently linked to glutamine residues of TG2 substrate proteins. The biotin group is then easily detectable by western blot using streptavidin coupled to horseradish peroxidase (HRP) (Lee, Maxwell et al., 1992). This procedure was applied to HeLa cells infected or not for 48 h with *C. trachomatis*. In non-infected samples, BP incorporation was extremely low, as expected since in resting cells low  $\text{Ca}^{2+}$  concentration maintains TG2 in an inactive conformation (Gundemir et al., 2012). In contrast, infected cells showed a significant incorporation of BP. CP4d, an inhibitor of TG2 transamidating activity (Caron, Munsie et al., 2012), abolished BP incorporation in a dose-dependent manner, indicating that BP incorporation was the result of the transamidase activity of TG2 (Fig. 1A). Live proliferating bacteria were needed for TG2 activation since filtered or heat-inactivated bacteria, or bacteria treated with the antibiotic doxycycline immediately after infection to prevent their proliferation, failed to induce BP incorporation (Fig. 1B and Fig. S1). BP incorporation upon infection was also observed in wild type mouse embryonic fibroblasts (MEFs) but not in MEFs isolated from *tgm2* knocked-out animals ( $\text{TG2}^{-/-}$ ), further supporting the implication of TG2 in this process (Fig. 1C).

Probing cellular lysates using anti-TG2 antibodies showed that activation of TG2 was accompanied with an increased expression of the enzyme (Fig. 1D). Consistent with this observation, inhibition of protein synthesis with cycloheximide decreased infection-induced BP incorporation (Fig. 1B). Reverse transcription followed by quantitative PCR (RT-qPCR) measurements revealed a 3- to 4-fold increase in the *TGM2* gene transcripts in infected versus non-infected cells, demonstrating that the increase in TG2 amount during infection is at least partly controlled at the transcriptional level (Fig. 1E). Interestingly, a positive feedback loop controls in part TG2 expression since *TGM2* transcription was no longer enhanced by infection when cells were treated with CP4d (Fig. 1E). *TGM2* transcription responds to a number of external stimuli including retinoic acid, hypoxia, and inflammatory cytokines such as IL-6 (Eckert et al., 2014, Suto, Ikura et al., 1993). We reasoned that IL-6 might be implicated in the transcriptional up-regulation of TG2 in *Chlamydia* infected cells as this cytokine is produced during infection (Rasmussen et al., 1997). We first verified that *TGM2* transcription showed a dose-dependent response to the addition of recombinant IL-6 in the culture medium (Fig. 1F). To test if IL-6 contributes to the transcriptional up-regulation of *TGM2* during infection we next performed the infection in the presence of anti-IL-6 receptor antibodies. We observed a reduction of *TGM2* transcription in infected cells with increasing concentrations of antibodies in the culture medium (Fig. 1G). Altogether, these data indicate that the induction of *TGM2* transcription in *C. trachomatis* infected cells is at least in part a consequence of IL-6 secretion in response to infection, followed by signaling through the IL-6 receptor.

In conclusion, *C. trachomatis* infection increases TG2 levels and activates its transamidase activity.

### **TG2 activity sustains bacterial growth**

To determine if TG2 activity affected bacterial development, we infected HeLa cells in the presence or not of the transamidase inhibitor CP4d. Thirty hours later, the progeny was collected and the number of infectious bacteria was determined by infecting fresh cells. Inhibition of TG2 activity with 40  $\mu$ M CP4d resulted in a 2-fold decrease in bacterial progeny (Fig. 2A). Consistently, a similar reduction in bacterial progeny was observed when TG2 activity was inhibited by cysteamine, another less specific inhibitor of TG2 (Figure EV1A). Progeny was also reduced when the bacteria were grown on TG2<sup>-/-</sup> MEFs compared to TG2<sup>+/+</sup>, indicating that the effect we had observed with TG2 inhibitors was not due to a direct toxicity of CP4d or cysteamine on the bacteria (Fig. EV1B). Consistent with these observations, silencing TG2 expression with two different siRNA resulted in up to a 3-fold decrease in progeny (Fig. 2B). To confirm these findings in primary cells, we used epithelial cells isolated from fallopian tubes (Roth, König et al., 2010). CP4d was even more potent at reducing the progeny after one developmental cycle in these cells than in HeLa cells, as a ten-fold reduction was observed for 10  $\mu$ M CP4d (Fig. 2C). The negative impact of TG2 inhibition on bacterial development was also observed in primary cells infected with *C. trachomatis* serovar D, showing that the effect is not restricted to the LGV biovar (Fig. 2C).

Reduced progeny could result from impairment of one or several of the steps of the chlamydial developmental cycle: adhesion, entry, differentiation into the replicative form, proliferation, and differentiation into the infectious form. We observed that the absence of TG2 in TG2<sup>-/-</sup> MEFs had no effect on bacterial adhesion (Fig. EV1C), but that it decreased the efficiency of bacterial internalization (Fig. EV1D). Consistently, 40  $\mu$ M CP4d decreased the percentage of infected cells by about 2-fold in HeLa cells (Fig. 2D). In addition, inclusions were smaller in cells treated with CP4d, and contained less bacteria, indicating that bacterial growth was slower in the absence of TG2 activity (Fig. 2D). The reduction of inclusion size when TG2 was inhibited was also observed in primary cells infected with *C. trachomatis* L2 or serovar D (Fig. 2E).

We next tested the incidence of the absence of TG2 on chlamydial development in a mouse model of infection. *Chlamydia muridarum* is a mouse-adapted strain genetically very close to *C. trachomatis* (Read, Brunham et al., 2000). Infection of HeLa cells with *C. muridarum* also activated TG2 (Fig. EV2A), and we observed the same effect of silencing TG2 on *C. muridarum* growth as on *C. trachomatis* (Fig. EV2B). We infected TG2<sup>+/+</sup> and TG2<sup>-/-</sup> mice intravaginally with *C. muridarum* and 25 days after infection, mice were sacrificed and the genital tract was isolated (Fig. 2F). DNA was extracted from the upper genital tract and bacterial load was determined by qPCR. A slightly higher number of mice retained detectable bacterial DNA in the wild type group (10/16, 62 %, for the TG2<sup>+/+</sup> and 4/9, 44% for the TG2<sup>-/-</sup> mice). Among the animals in which bacterial DNA was still detected, the trend was for a higher bacterial load in the wild type background, but the number of TG2<sup>-/-</sup> animals we could breed

was too low for statistical significance. These data indicate that the absence of TG2 reduces only marginally, if at all, the ability for *C. muridarum* to establish an infection. It is however possible that in some tissues the loss of TG2 is compensated by expression of other transglutaminases, limiting the interpretation of these data (Iismaa et al., 2009). One clear difference between the two groups came from anatomical observations: TG2<sup>-/-</sup> animals showed milder signs of inflammation than their wild type littermate, especially when the oviduct hydrosalpinx scores were compared. It thus appears that the presence of TG2 exacerbates the tissue damage in this mouse model of infection, in line with the implication of TG2 in tissue fibrosis (Eckert et al., 2014, Iismaa et al., 2009).

### **TG2 plays a central role in metabolic rewiring**

We have recently shown that *C. trachomatis* acts as a glucose sink (Gehre et al., 2016). The host cell responds to glucose demand by increasing glucose uptake through overexpression of plasma membrane glucose transporters (Ojcius, Degani et al., 1998, Wang, Hybiske et al., 2017). Since we observed that TG2 level was increased during *C. trachomatis* infection, we wondered if this increase could control the concomitant increase in glucose transporter expression, as it does in mammary epithelial cells (Kumar, Donti et al., 2014). If this hypothesis was correct, one prediction that we could make was that low glucose availability in the culture medium should be more detrimental to bacterial growth in TG2<sup>-/-</sup> MEFs compared to the wild type MEFs, as TG2<sup>-/-</sup> MEFs would be impaired in their ability to adjust their glucose uptake to sustain bacterial growth. To test this hypothesis, we grew MEFs in medium containing decreasing concentrations of glucose and measured the number of infectious bacteria collected 30 hpi. As expected we observed that decreasing glucose availability resulted in a sharp decrease in bacterial titers, in both cellular backgrounds. However, bacterial titers were more sensitive to glucose deprivation in the TG2<sup>-/-</sup> MEFs than in the wild-type cells (Fig. 3A). For instance, at 1 mg/mL glucose, the progeny was reduced by 82% in the TG2<sup>-/-</sup> MEFs, compared to only 35% in the TG2<sup>+/+</sup> MEFs.

To test the implication of TG2 in the rewiring of host metabolism more directly, we measured the incidence of TG2 inactivation on the cell capacity to uptake glucose. HeLa cells infected with *C. trachomatis* show increased transcription of *GLUT-1* and *GLUT-3*, which allows to increase glucose uptake and meet bacterial needs (Wang et al., 2017). We reproduced this result in HeLa cells, as well as in primary cells isolated from the endocervix (Fig. 3B). In contrast, in the presence of the TG2 inhibitor CP4d, the transcription of the glucose transporter genes was no longer induced by infection, indicating that TG2 is necessary for the control of *GLUT-1* and *GLUT-3* transcription. Absence of increase in *GLUT-1* and *GLUT-3* transcripts 48 hpi in the presence of CP4d was not due to the lower bacterial burden because when bacterial proliferation was interrupted 24 hpi by addition of doxycycline we observed a comparable reduction in bacterial load at 48 hpi as in cells treated with CP4d, but the transcription of the glucose transporter genes remained as high as in non-treated cells (Fig. S2).

Finally, to explore further the incidence of TG2 expression on that of glucose transporters we examined transcriptional data from a cohort of high grade serous ovarian cancer (HGSOC) patients. This population was chosen because clinical and biological data indicate that TG2 overexpression is an adverse prognostic factor in ovarian carcinoma (Hwang, Mangala et al., 2008, Shao, Cao et al., 2009). We observed a significant correlation between expression of *TGM2* and *GLUT-3* across the 265 clinical HGSOC specimens ( $p=0.50$ ,  $P<0.001$ ) (Fig.3C). The HGSOC cohort also demonstrated significant correlation between TG2 and GLUT-1 expression, though the magnitude of correlation was less marked ( $p=0.21$ ,  $P<0.001$ ) (Fig. 3C). Collectively, these data support the notion that TG2 plays a central role in regulating glucose transporters expression regulation in the context of infection or malignancy, thereby playing a central role in the control of the metabolic balance.

### **The hypoxia-inducible factor 1 and the transamidase activity of TG2 are required for the transcriptional up-regulation of glucose transporters**

One major transcriptional regulator of the expression of glucose transporters is the hypoxia-inducible factor 1 (HIF-1), which is increased during *Chlamydia* infection (Sharma, Machuy et al., 2011). Infection did not result in an increase in HIF-1 $\alpha$  transcripts, indicating that the increase in HIF-1  $\alpha$  occurs by stabilization of the transcription factor (Fig. 3D). To test whether HIF-1 was implicated in infection-induced up-regulation of glucose transport we silenced HIF-1 $\alpha$  expression before infecting the cells. Under these conditions, we observed a loss of induction of *GLUT-1* and *GLUT-3* transcription in infected cells. In contrast, the increase in *TGM2* transcripts upon infection remained, placing HIF-1 $\alpha$  downstream of *TGM2* induction (Fig. 3E).

In the presence of the TG2 inhibitor CP4d, the transcription of the glucose transporter genes was no longer induced by infection (Fig. 3B), indicating that the transamidase activity of TG2 was required. However, this observation could also be accounted for by the inhibition that CP4d exerts on TG2 expression in infection (Fig. 1E). To address directly the role of TG2 transamidase activity in the regulation of the expression of glucose transporter genes we used TG2<sup>-/-</sup> MEFS in which TG2 wild-type or mutated for the transamidase activity (C277S mutant) were constitutively expressed (Rossin, D'Eletto et al., 2012). We focused on the regulation of *GLUT-1*, as we did not observe an increase in *GLUT-3* expression upon infection in this cellular background. Consistently with our previous findings, infection failed to induce an increase in *GLUT-1* transcripts in TG2<sup>-/-</sup> MEFS (Fig. 3F). Constitutive expression of wild-type TG2, but not of the C277S mutant, restored the induction of *GLUT-1* transcription upon infection. This observation demonstrates that the transamidase activity of TG2 is required for the increase in *GLUT-1* transcription upon infection.

Altogether, these data show that the transcription factor HIF-1, and TG2 transamidating activity, are both required for the up-regulation of glucose transporters during *C. trachomatis* infection.

### **TG2 targets glutamine:fructose-6-P amidotransferase and enhances its activity**



In addition to its role in the up-regulation of the transcription of glucose transporter genes, TG2 may confer other benefits to *C. trachomatis*. To identify TG2 targets in the infectious process, HeLa cells were infected in the presence or absence of BP. Forty-eight hours later the cells were lysed and biotinylated proteins were isolated on streptavidin-coated beads, and identified by mass-spectrometry. Sixty-two proteins were found to be significantly enriched in the infected cell lysates grown in the presence of BP (Table S1). Fibronectin, galectin 3, RhoA, 40S ribosomal protein SA, immunoglobulin  $\kappa$  chain C region and hemoglobin beta were already identified as TG2 substrates (Guilluy, Rolli-Derkinderen et al., 2007, Mehul, Bawumia et al., 1995, Nelea, Nakano et al., 2008, Orrù, Caputo et al., 2003, Pincus & Waelsch, 1968, Sohn, Chae et al., 2010). BAG2 and several other mitochondrial proteins were also enriched in the samples prepared in the presence of BP, in agreement with TG2 being present and active in this compartment (Altuntas, Rossin et al., 2015).

Among the potential TG2 substrates we identified in *C. trachomatis* infected cells, the enzyme glutamine:fructose-6-P amidotransferase (GFPT) caught our attention because it uses fructose-6-P as a substrate, which is derived from glucose-6-P. Moreover, both isoforms of the enzyme, GFPT1 (also called GFAT) and GFPT2, had been recovered from the proteomic approach, making it a very strong hit. We first confirmed that GFPT was recovered in the biotinylated fraction of cells infected with *C. trachomatis* in the presence of BP using anti-GFPT antibodies. The abundance of GFPT in the biotinylated fraction strongly decreased when infection had been performed in the presence of the TG2 inhibitor CP4d, demonstrating that incorporation of the biotinylated probe in GFPT depended on the activity of TG2 (Fig. 4A).

To further validate that GFPT is a novel substrate of TG2, purified TG2 and recombinant human GFPT1 (rhGFPT1) were incubated for 3 h at 37 °C in the presence of BP as primary amine donor. The incorporation of the biotinylated probe was analyzed by blotting with HRP-coupled streptavidin. The biotinylated probe was incorporated into rhGFPT1 in the presence and not in the absence of TG2. Furthermore, chelation of  $\text{Ca}^{2+}$  by EGTA inhibited the incorporation of the probe, as expected for a reaction dependent on the transamidase activity of TG2 (Fig. 4B). We concluded from these experiments that GFPT is a novel substrate of TG2 that becomes modified by the transamidase activity of the enzyme during *C. trachomatis* infection.

In order to determine which glutamine residue(s) of GFPT1 was modified by TG2 *in vitro*, we analyzed the products of the reaction by mass spectrometry. BP incorporation was identified in ten glutamine residues (out of twenty-eight, Fig. 4C), presumably because promiscuous reactions occur *in vitro*. Among those, two glutamine residues were identified as prone to modification by TG2 using bioinformatics tools designed to score the peptidic environment favorable for TG2 activity, namely Q328 and Q555 (Keresztessy, Csosz et al., 2006, Sugimura, Hosono et al., 2006). We thus generated a glutamine to asparagine point mutant for each of these residues to minimize the impact on protein folding. As a control, we also mutated Q58, another candidate target identified by mass spectrometry but not surrounded by a consensus sequence for TG2. Purified recombinant proteins were incubated with TG2 and BP for 30 min at 37 °C before stopping the reaction. BP incorporation was

significantly reduced only in the rhGFPT1 Q328N, indicating that the Q328 is a prominent glutamine for modification by TG2 (Fig. 4D).

The fact that *C. trachomatis* produce their own GFPT (named GlmS) prevented us from measuring the consequence of TG2 activation on host GFPT activity in infected cells. However, ionomycin is a widely used TG2 activator, as this  $\text{Ca}^{2+}$  ionophore increases intracellular  $\text{Ca}^{2+}$  concentration, which opens TG2 in its active conformation. We thus measured GFPT activity in lysates of cells treated or not with ionomycin, and analyzed the reaction products by high performance anion exchange chromatography (Fig. S3). We observed a three-fold increase in GFPT activity in cells treated with ionomycin, indicating that GFPT modification by TG2 increases the activity of the enzyme (Fig. 4E).

### **Modification of GFPT by TG2 enhances the hexosamine biosynthesis pathway**

The reaction catalyzed by GFPT is the first and rate limiting step of the hexosamine biosynthesis pathway (HBP, Fig. 5A). The HBP leads to the formation of uridine 5'-diphospho-*N*-acetylglucosamine (UDP-GlcNAc), which is further used for *N*-glycosylation, *N*-glycan branching, and *O*-linked *N*-acetylglucosylation (*O*-GlcNAcylation) in the ER, Golgi, and nucleus/cytosol, respectively. *O*-GlcNAcylation involves the transfer of a single UDP-GlcNAc moiety to the hydroxyl groups of serine or threonine residues. Two enzymes, *O*-GlcNAc transferase (OGT) and *O*-GlcNAc case (OGA), catalyze *O*-GlcNAc addition and removal, respectively and the *O*-GlcNAc modification level of proteins is directly dependent on the concentration of UDP-GlcNAc, the donor substrate for OGT (Kreppel & Hart, 1999). To confirm that GFPT modification by TG2 increased its activity and thus hexosamine biosynthesis we measured the level of *O*-GlcNAcylation in primary epithelial cells. We observed an increase in *O*-GlcNAcylation in cells treated with ionomycin. This increase was dependent on TG2 activity since it was not observed in the presence of the TG2 inhibitor CP4d (Fig. 5B) or in cells in which *TGM2* expression had been silenced using siRNA (Fig. 5C). Altogether these experiments show that activation of TG2 transamidase activity enhances the HBP.

### **The increase in the hexosamine biosynthetic pathway is hijacked by the bacteria**

Surprisingly, we did not observe an increase in *O*-GlcNAcylation in cells infected for 48 h by *C. trachomatis* (Fig. 6A). Since *O*-GlcNAcylation directly depends on UDP-GlcNAc concentration this observation suggests that UDP-GlcNAc levels in the cytoplasm are not significantly increased in infected cells. We have previously demonstrated that *C. trachomatis* co-opts SLC35D2, a host antiporter transporting UDP-GlcNAc, UDP-glucose and GDP-mannose to import these metabolites into the vacuole in which the bacteria develop (Gehre et al., 2016). We reasoned that UDP-GlcNAc might not accumulate in the cytoplasm in infected cells because it was relocated to the inclusion lumen. Supporting this hypothesis, we observed that activation of TG2 by ionomycin elicited a lower increase in *O*-GlcNAcylation in infected cells compared to non-infected cells, indicating that less free UDP-GlcNAc is available for *O*-GlcNAcylation in the infected host cytoplasm (Fig. 6B). Importantly GFPT expression was

stable in all conditions, indicating that the decrease in *O*-GlcNAcylation in infected cells is not due to lower GFPT expression (Fig. 6A-B).

In Gram-negative bacteria, UDP-GlcNAc supply is mostly used for lipopolysaccharide and peptidoglycan biosynthesis. *C. trachomatis* do not have a classical cell wall but use peptidoglycan synthesis for bacterial division (Liechti, Kuru et al., 2016). If UDP-GlcNAc, or an intermediate along the hexosamine biosynthesis pathway, was consumed at least partly in making bacterial peptidoglycan, lowering hexosamine biosynthesis should delay bacterial division, resulting in larger bacteria being formed. We tested this hypothesis by measuring the consequence of silencing GFPT, the rate-limiting enzyme in hexosamine biosynthesis, on bacterial size. The mass spectrometry data showed that both isoforms GFPT1 and GFPT2 were expressed in HeLa cells (Table S1). Comparison of the efficiency of siRNA designed to target specifically one isoform showed that GFPT2 was hardly detectable and targeting GFPT1 was sufficient to strongly decrease GFPT expression (Fig. 6C). We thus lowered hexosamine biosynthesis by treating cells with a siRNA against GFPT1 prior to infection, fixed the cells at increasing time of infection and used flow cytometry to measure bacterial sizes. As expected, the number of replicative bacteria increased with infection time (Fig. S4). Furthermore, it was recently demonstrated that replicative bacteria gradually decrease in size over the course of the developmental cycle (Lee, Enciso et al., 2017). We indeed observed a decrease in bacterial diameter over a 20 to 26 hpi time course, thereby validating the use of flow cytometry to measure the size of *C. trachomatis* (Fig. S4 and 6D). In cells treated with a siRNA against GFPT1 the mean bacterial diameter became significantly higher than in control cells 24 hpi (Fig. 6D). We confirmed this result by measuring the diameter of bacteria on electron microscopy pictures of cells infected for 30 h (Fig. EV3). These kinetics fit well with our observation that TG2 activity increases between 24 and 48 hpi, when bacterial load is high, and access to nutrients might become limiting (Rother, Gonzalez et al., 2018). These observations support the hypothesis that a product of the hexosamine biosynthesis pathway is captured by the inclusion to support division. Consistent with a role for GFPT activity in sustaining bacterial growth we observed a reduction in the number of bacteria per inclusion 24 h post infection in the cells treated with siRNA against GFPT1, and the progeny collected was reduced 3-fold (Fig. 6E). Of note, silencing of GFPT1 had no incidence on bacterial entry and the initiation of bacterial development, as the percentage of infected cells was identical to that in control cells (Fig. 6E). Altogether, these data strongly support the hypothesis that the increase in hexosamine biosynthesis by the host upon GFPT modification by TG2 is exploited by the bacteria, in particular to assist bacterial division. Interestingly, we observed that silencing TG2 also increased bacterial size (Fig. 6D). While silencing TG2 has multiple effects beyond harnessing the HBP, these data are fully consistent with GFPT activation being one of the major outcomes of TG2 upregulation during *C. trachomatis* infection.

## DISCUSSION

TG2 transamidase activity is very potent, and would be deleterious if not tightly controlled. In basal conditions it is mostly turned off, and it is thought that under specific stress conditions, the enzyme might be locally turned on and transamidate specific substrates. The infection with *C. trachomatis* provided a unique physiological situation where the expression and activity of the enzyme were increased over a relatively short period of time in a physiological set-up. We took advantage of this observation to identify TG2 substrates. Among the 62 candidates identified, we focused on the enzyme GFPT. We showed that GFPT modification by TG2 increased its activity, resulting in higher hexosamine biosynthesis, a process also fueled by the positive control exerted by TG2 on glucose transporters expression. The product of the HBP, UDP-GlcNAc, is used for post-translational modification of proteins by *O*-GlcNAcylation. Thus, our work uncovered an unsuspected link between TG2 transamidase activity and *O*-GlcNAcylation. This link was disrupted in infected cells because the increase in hexosamine biosynthesis in the host was exploited by the bacteria, in particular to assist their division. In conclusion, our work establishes TG2 as a key player in controlling glucose-derived metabolic pathways in mammalian cells, themselves hijacked by *C. trachomatis* to sustain their own metabolic needs (Fig. 6F).

Several inflammatory conditions are associated with an increase in TG2 expression (Eckert et al., 2014). We confirmed that IL-6 up-regulates *TGM2* transcription (Eckert et al., 2014, Suto et al., 1993) and we showed that this cytokine is implicated in the increase in *TGM2* transcription during *C. trachomatis* infection (Rasmussen et al., 1997) since anti-IL-6 receptor antibodies antagonized the induction of TG2 expression. How the enzyme becomes activated is less clear. In the cell  $\text{Ca}^{2+}$  concentration is high in the endoplasmic reticulum, and this compartment is tightly associated to the inclusion membrane (Derré, Swiss et al., 2011). The unfolded protein response pathway is activated in infected cells (George, Omosun et al., 2016), a condition that might be sufficient to activate TG2 (Lee, Jeong et al., 2014). Indeed accumulation of cytoplasmic  $\text{Ca}^{2+}$  around the inclusion has been reported (Majeed, Krause et al., 1999), which might be enough to locally activate TG2.

Treatment of cells with a potent inhibitor of TG2, CP4d, reduced progeny ten-fold in primary epithelial cells (Fig. 2). We have shown that the inhibition of TG2 activity had two distinct effects on *C. trachomatis* developmental cycle. First, it reduced the ability for the bacteria to enter the cells (Fig. S2). *C. trachomatis* use multiple receptors and appear to hijack several entry pathways into epithelial cells (Ford, Nans et al., 2018). The positive role played by TG2 on bacterial entry, which could be exerted from its intracellular or extracellular location, remains to be studied in future work. One attractive candidate mechanism is PDGFR signaling, since it is implicated in *C. trachomatis* entry (Elwell, Ceesay et al., 2008) and it is sensitive to TG2 activity (Nurminskaya, Beazley et al., 2014). Second, the inclusion developed slower in CP4d-treated culture, indicating that TG2 is necessary for optimal bacterial growth. We discuss below the two mechanisms we uncovered that account for the link between TG2 activation and bacterial development, and place TG2 as a key regulator of bacterial access to glucose and its derivative UDP-GlcNAc.

We have shown that TG2 is required for the increase in transcription of *GLUT-1* and *GLUT-3* in infection in HeLa cells and in primary epithelial cells (Fig. 2). Glucose is an essential metabolite for *C. trachomatis* development and preventing the transcription of *GLUT-1* and *GLUT-3* by siRNA led to a two-fold decrease in progeny in HeLa cells (Wang et al., 2017). This result shows that glucose import can become limiting for bacterial growth, and thus that the control exerted by TG2 on the expression of glucose transporters accounts, at least in part, for the need for this enzyme for optimal bacterial growth. This conclusion is supported by our observation that glucose becomes limiting faster for bacterial progeny in MEFs lacking TG2 than in wild-type cells. Thus, our study places TG2 as a key regulator for glucose import in infected cells.

Mechanistically, we showed that HIF-1 was required for *Chlamydia*-induced increase in the transcription of glucose transporters. HIF-1 $\alpha$  transcription does not increase during infection. TG2 interacts with HIF-1 $\beta$  (Filiano, Bailey et al., 2008), and an increase in TG2 levels upon infection might be sufficient to stabilize the HIF-1 complex. It is however not sufficient to account for infection-induced up-regulation of glucose transporters since we demonstrated that the transamidating activity of TG2 was required in this context. Through a series of elegant experiments the Johnson lab showed that the effect of TG2 on transcription was highly cell and context dependent (Gundemir, Colak et al., 2013, Gundemir, Monteagudo et al., 2017). TG2 modifies several transcription factors (Gundemir et al., 2012), but none of these known targets were recovered in our proteomic approach for the identification of TG2 targets upon infection. Furthermore, it was shown very recently that TG2 enhanced chromatin binding of the general transcription factor complex TFIID through the serotonylation of histone 3 trimethylated lysine 4 (Farrelly, Thompson et al., 2019). This, or another transglutaminase-mediated histone modification, might be implicated in the transcriptional control of glucose transporter genes in the infectious context.

Our proteomic approach identified 62 candidate TG2 substrates in *C. trachomatis* infection. Six of those were already known substrates of TG2, validating our analysis. We further demonstrated that GFPT was a substrate of TG2 and identified Q328 as a prominent transamidation site. The absence of shift in the migration profile of GFPT suggests that the amine donor is either a small protein, or a small amine, or that deamidation occurs, making identification by mass spectrometry very challenging. Experiments on GFPT immunoprecipitated from ionomycin-treated samples failed to detect histaminylation or serotonylation. Deamidation was occasionally seen on several glutamine residues, including Q328, raising questions as to the relevance of this observation that will be addressed in future studies.

We showed that GFPT activity was enhanced upon transamidation by TG2. This resulted in an increase in *O*-GlcNAcylation, since this post-translational modification of proteins is directly dependent on the concentration of UDP-GlcNAc (Kreppel & Hart, 1999). GFPT acts as a tetramer and is negatively regulated by several post-translational modifications (Chang, Su et al., 2000, Zibrova, Vandermoere et al., 2017) and by UDP-GlcNAc (Assrir, Richez et al., 2014).

Transamidation on Gln328 could interfere with these down-regulation mechanisms and thereby unleash the HBP.

Interestingly the positive correlation between TG2 activation and *O*-GlcNAcylation does not hold true in infected cells and our data indicate that this is due to hexosamines being consumed by the infection. Our observation that silencing GFPT expression increases bacterial diameter strongly supports the hypothesis that UDP-GlcNAc, or an intermediate along the HBP, is hijacked into the inclusion to fuel bacterial division, possibly by feeding peptidoglycan synthesis. Interestingly, a proximity-based labeling assay recently described an enrichment of TG2 and GFPT1 around the inclusion, suggesting that TG2 activation and GFPT modification might be most efficient in proximity of the bacteria-containing compartment (Olson, Widner et al., 2019). One recent publication showed that UDP-GlcNAc is also used during infection to post-translationally modify the intermediate filament vimentin and this also could contribute to significant UDP-GlcNAc consumption in *C. trachomatis* infection (Tarbet, Dolat et al., 2018).

The role played by TG2 in viral or microbial infections is raising increasing interest. Like in the case of *C. trachomatis* infection, genetic or pharmacological inhibition of TG2 led to a marked reduction in *Mycobacterium tuberculosis* replicative capacity. However, the mechanism involved might be different, since the data suggest that reduced replication in macrophages lacking TG2 is due to the impairment of autophagy homeostasis (Palucci, Matic et al., 2017). *M. tuberculosis* relies largely on lipids and fatty acids as energy source, and glucose availability might not be limiting in this case (Russell, VanderVen et al., 2010). Still, up-regulation of glucose transporter was also described in a mouse model of *M. tuberculosis* infection (Shi, Salamon et al., 2015), thus the involvement of TG2 in metabolism regulation in this context remains to be investigated.

There are multiple examples of host manipulation by pathogens that shed light on fundamental cellular processes. Here our work revealed an unsuspected regulation of the HBP by TG2. This discovery has important implications. Like other post-translational modifications, protein *O*-GlcNAcylation dramatically alters the fate and function of target proteins. In particular transcription factors are modified by *O*-GlcNAcylation, which implicates this modification in transcriptional regulation (Jackson & Tjian, 1988). Physiologically, disruption of *O*-GlcNAcylation homeostasis has been implicated in the pathogenesis of many human diseases, which include cancer, diabetes and neurodegeneration (Jóźwiak, Forma et al., 2014, Yang & Qian, 2017). The link between TG2 and *O*-GlcNAcylation means that TG2 activation is expected to have broad transcriptional consequences. In particular TG2 is activated in many cancers and future investigation is required to determine the contribution of the TG2/GFPT activation axis to tumorigenesis.

## MATERIAL AND METHODS

### Cells and bacteria

HeLa cells (ATCC) and mouse embryonic fibroblasts (MEFs) isolated from KO (TG2<sup>-/-</sup>) or WT (TG2<sup>+/+</sup>) C57B6 mice, were grown in Dulbecco's modified Eagle's medium with Glutamax

(DMEM, Invitrogen), supplemented with 10 % (v/v) heat-inactivated fetal bovine serum (FBS) (D'Eletto, Farrace et al., 2009). TG2<sup>-/-</sup> cells reconstituted with stable expression of wild type or C277S TG2 are described in (Rossin et al., 2012). Primary cells used for experiments displayed in Fig. 2 were isolated from human fallopian tubes and maintained in culture as previously described (Roth et al., 2010). Other primary cells were isolated from endocervix biopsies of female patients and were cultivated in keratinocyte-SFM medium (Thermo Fisher Scientific) containing 50 mg.L<sup>-1</sup> of bovine pituitary extract (Thermo Fisher Scientific) and 5 µg.L<sup>-1</sup> of epidermal growth factor (EGF) human recombinant (Thermo Fisher Scientific) (Wu *et al*, in preparation). All cell cultures were maintained at 37 °C, in 5 % CO<sub>2</sub> atmosphere and were routinely tested for mycoplasma using the standard PCR method. *C. trachomatis* serovar LGV L2 strain 434 and serovar D/UW-3/CX (ATCC), GFP-expressing L2 (L2<sup>IncD</sup>GFP) or *C. muridarum* MoPn (for *in vivo* experiments) were propagated on HeLa cells, purified on density gradients as previously described and stored at -80 °C (Scidmore, 2005, Vromman, Laverriere et al., 2014).

#### siRNA treatment

For siRNA experiments, 50 000 cells were plated in a 24-well plate and immediately mixed with Lipofectamine RNAiMAX (Invitrogen) following the manufacturer's recommendation, using 10 nM of siRNA (Table S2). For RB size assessment, 300 000 cells were plated in a 6-well plate. For electron microscopy experiments, 1.5 million cells were plated in a 25-cm<sup>2</sup> flask. For GFPT1 activity assay, 1 million cells were plated in a 10-cm diameter dish. The culture medium was changed the next day and experiments (infection or treatment with ionomycin) were performed two days post treatment with the siRNA.

#### GFPT1 purification

Recombinant human GFPT1 (rhGFPT1) with an internal 6-His tag was produced from a plasmid pET28-rhGFPT1-6His in *E. coli* Rosetta (DE3) GlmS::Tc kindly given by Dr. Badet-Denisot (Centre de Recherche de Gif, France) (Li, Roux et al., 2007). The mutated form rhGFPT1 Q58N, rhGFPT1 Q328N and rhGFPT1 Q555N were obtained using QuikChange technology (Agilent) on the plasmid pET28-rhGFPT1-6His, with primers listed in Table S2, following the manufacturer instructions, and transformed in *E. coli* Rosetta (DE3) GlmS::Tc.

One litre of culture in 2YT medium supplemented with tetracycline (8 µg.mL<sup>-1</sup>, Sigma), kanamycin (50 µg.mL<sup>-1</sup>, Sigma), chloramphenicol (15 µg.mL<sup>-1</sup>, Sigma) and glucosamine (GlcNH<sub>2</sub>, 2 mg.mL<sup>-1</sup>, Sigma) was incubated with agitation at 37 °C until OD<sub>600</sub> reached 0.5. Protein expression was induced by addition of 0.5 mM of isopropyl β-D-thiogalactopyranoside (Sigma) at 25 °C for 24 h before being harvested. The cell pellets were resuspended in lysis buffer (16.27 mM Na<sub>2</sub>HPO<sub>4</sub> and 3.73 mM NaH<sub>2</sub>PO<sub>4</sub> pH 7.5, 200 mM NaCl, 20 mM imidazole, 2 mM tris(2-carboxyethyl)phosphine hydrochloride (TCEP), 10 % glycerol, 1 mM fructose-6-P, Roche EDTA-free protease inhibitor cocktail) and disrupted by sonication. The recombinant protein was purified by incubation with Qiagen Ni-NTA agarose beads (Qiagen) for 1 h followed by three washing steps with the lysis buffer before elution with lysis buffer containing increasing concentrations of imidazole: 30 mM, 100 mM, 175 mM and finally 500 mM of imidazole. The fractions containing the protein were dialyzed against lysis buffer with 20 mM HEPES replacing the phosphate buffer before storage at -80 °C

#### TG2 activity assay

*In vivo*: Cells plated the day before (100 000 cells/well) were infected with *C. trachomatis* serovar LGV L2 at a MOI of 1, and 0.5  $\mu$ M biotin pentylamine (BP) (Thermo Fisher Scientific) was added after 24 h. In some experiments, cells were pre-incubated for 2 h with 40  $\mu$ M CP4d or DMSO as control before addition of bacteria. CP4d inhibits the transamidase activity of TG2 ( $K_i$  = 174 nM) and favours its closed conformation (Caron et al., 2012). For experiments with ionomycin (Sigma), cells pre-treated with siRNA for 48 h or infected as described above for 24 h were treated with Ionomycin and 0.5  $\mu$ M BP for 6 h.

At the end of the indicated incubation time, cells were lysed using 8 M urea buffer (30 mM Tris, 150 mM NaCl, 8 M urea, 1 % SDS, pH=8.0) and samples subjected to Western Blot.

*In vitro*: 1 mU of transglutaminase from guinea pig liver (Sigma) was incubated at 37 °C for 15 min or 3 h with 5  $\mu$ g of rhGFPT1, rhGFPT1 Q58N or rhGFPT1 Q328N and 1 mM of BP in 20 mM HEPES buffer pH 7.5, 200 mM NaCl, 2 mM TCEP, 10 % glycerol, 1 mM fructose-6-phosphate, 10 mM  $\text{CaCl}_2$ . The reaction was stopped by adding ethylene-bis(oxyethylenenitrilo)tetraacetic acid (EGTA) at a final concentration of 20 mM and boiling the samples 5 min at 95 °C.

### **Streptavidin-precipitation of TG2 targets**

Twenty million HeLa cells were seeded in a 163-cm<sup>2</sup> flask. One day later, the cells were infected or not with *C. trachomatis* serovar LGV L2 at a MOI = 1. Two hours post infection (hpi) the culture medium was changed and 40  $\mu$ M CP4d or DMSO was added. BP was added to the culture medium at 0.5 mM 24 h post treatment (infection or not) and cells were lysed 46 hpi directly in the well using 8 M urea buffer. DNA was disrupted by sonication and a dialysis was performed against 2 M urea buffer (Tris 30 mM, NaCl 150 mM, 2 M urea, 1 % SDS, pH=8.0). Samples were incubated overnight at 4 °C with streptavidin-agarose beads (Sigma). After 3 washes with 2 M urea buffer and 3 washes with phosphate-buffered saline (PBS), proteins precipitated on the beads were eluted using Laemmli's buffer containing dithiothreitol (Sigma) boiled 5 min at 95 °C. Samples were then analyzed by Western blot or by mass spectrometry.

### **SDS-PAGE and Western blot**

Proteins were subjected to sodium dodecyl-sulfate polyacrylamide gel electrophoresis (SDS-PAGE) and transferred to a polyvinylidene difluoride (PVDF) membrane, which was blocked with 1 x PBS containing 5 % bovine serum albumin (BSA, for biotin revelation only) or milk and 0.01 % Tween 20. The membranes were then immunoblotted with primary antibodies diluted in 1 x PBS containing 5 % milk and 0.01 % Tween 20. For analyzing the TG2 activity assay, biotin incorporation was revealed using streptavidin conjugated to HRP (#RPN1231, Sigma). Primary antibodies used in the western blots were the mouse clone 7D2 against TG2 (#ABIN1109303, Covalab), rabbit anti-serum against GFPT (kindly given by Dr. C. Weigert, University of Tübingen, Germany), mouse clone RL2 against O-GlcNAcylation (#MA1-072 Thermo Fisher Scientific) and mouse clone AC-74 against  $\beta$ -actin (#A5441 Sigma). Secondary antibodies were anti-mouse-HRP (#NA931, GE Healthcare) or anti-rabbit-HRP (#G-21234, Invitrogen) conjugated antibodies. Blots were developed using the Western Lightning Chemiluminescence Reagent (GE Healthcare).

### **Ovarian cancer cohort and statistical analysis**



Expression data for *TGM2*, *GLUT-1* and *GLUT-3* in 265 high grade serous ovarian cancers from Edinburgh were available from previous transcriptomic studies of ovarian cancer (Hollis, Churchman et al., 2019). Per-sample expression was calculated as the mean expression of probe-sets informative for each gene. Expression comparisons were performed using Spearman's rank correlation test. Spearman's rank correlation was chosen over Pearson's correlation following demonstration of non-normal expression distribution for *TG2*, *GLUT-1* and *GLUT-3* (Shapiro-wilk normality test,  $P < 0.05$  for all).

## Mass Spectrometry

*In solution protein digestion:* Samples were prepared in triplicate. For streptavidin-precipitation of *TG2* targets samples, tryptic digestion was performed by enhanced filter-aided sample preparation. All steps were done in-filter. Briefly, samples were reduced (50 mM TCEP, 30 minutes at room temperature) and alkylated (50 mM iodoacetamide, 1 h at room temperature in the dark). Then, proteins were incubated overnight at 37 °C with 500bng trypsin (Trypsin Gold Mass Spectrometry Grade, Promega). Peptides were recovered by centrifugation.

After *TG2*/*GFPT1* reactions *in vitro* samples were diluted in a large excess of 8 M urea / 100 mM Tris HCl pH 8.5 buffer and then, as previously described, reduced (5 mM TCEP, 30 minutes at room temperature) and alkylated (10 mM iodoacetamide, 30 minutes at room temperature in the dark). Proteins were first digested for 5 h at 37 °C with 500 ng rLys-C Mass Spec Grade (Promega, Madison, WI, USA) before being diluted 4-fold with 100 mM Tris HCl pH 8.5 to reach a concentration below 2 M urea. Samples were then incubated overnight at 37 °C with 500 ng Sequencing Grade Modified Trypsin (Promega, Madison, WI, USA). To achieve the complete digestion of the peptides, a second incubation with the same amount of trypsin (5 h at 37 °C) was performed. Digestion was stopped by adding formic acid to 5 % final concentration and peptides were desalted and concentrated on Sep-Pak C<sub>18</sub>SPE cartridge (Waters, Milford, MA, USA) according to manufacturer instructions.

*Mass spectrometry analysis:* Tryptic peptides were analyzed on a Q Exactive Plus instrument (Thermo Fisher Scientific, Bremen) coupled with an EASY nLC 1 000 or 1 200 chromatography system (Thermo Fisher Scientific, Bremen). Sample was loaded on an in-house packed 50 cm nano-HPLC column (75 µm inner diameter) with C<sub>18</sub> resin (1.9 µm particles, 100 Å pore size, Reprosil-Pur Basic C<sub>18</sub>-HD resin, Dr. Maisch GmbH, Ammerbuch-Entringen, Germany) and equilibrated in 98 % solvent A (H<sub>2</sub>O, 0.1 % FA) and 2 % solvent B (ACN, 0.1 % FA). 120 or 180 min gradient of solvent B at 250 nL.min<sup>-1</sup> flow rates were applied to separated peptides. The instrument method for the Q Exactive Plus was set up in DDA mode (Data Dependent Acquisition). After a survey scan in the Orbitrap (resolution 70 000), the 10 most intense precursor ions were selected for HCD fragmentation with a normalized collision energy set up to 28. Charge state screening was enabled, and precursors with unknown charge state or a charge state of 1 and > 7 were excluded. Dynamic exclusion was enabled for 35 or 45 seconds respectively.

*Data processing:* Data were searched using Andromeda with MaxQuant software 1.4.1.2 or 1.5.3.8 version against respectively a *Chlamydia trachomatis* Uniprot reference proteome database concatenated with Homo sapiens Uniprot reference proteome database. Data were also searched against usual known mass spectrometry contaminants and reversed sequences of all entries or an *E. coli* K12 Uniprot reference proteome database concatenated with

rhGFPT1 and gpTGase proteins (Tyanova, Temu et al., 2016). Andromeda searches were performed choosing trypsin as specific enzyme with a maximum number of two missed cleavages. Possible modifications included carbamidomethylation (Cys, fixed), oxidation (Met, variable), N-ter acetylation (variable) and BP (Gln, variable). The mass tolerance in MS was set to 20 ppm for the first search then 6 ppm for the main search and 10 ppm for the MS/MS. Maximum peptide charge was set to seven and five amino acids were required as minimum peptide length. The “match between runs” feature was applied between replicates with a maximal retention time window of 2 or 0.7 min. One unique peptide to the protein group was required for the protein identification. A false discovery rate (FDR) cutoff of 1 % was applied at the peptide and protein levels.

*Data analysis:* To validate the identification of the BP on the glutamine of modified peptides, spectra were manually inspected (or fragment assignments).

For the global quantification, output files from MaxQuant were used for protein quantification. Quantification was performed using the XIC-based LFQ algorithm with the Fast LFQ mode as described previously (Cox, Hein et al., 2014). Unique and razor peptides, included modified peptides, with at least 2 ratio count were accepted for quantification.

For pairwise comparisons, proteins identified in the reverse and contaminant databases and proteins only identified by site were first discarded from the list. Then, proteins exhibiting fewer than 2 LFQ values in at least one condition were discarded from the list to avoid misidentified proteins. After log2 transformation of the leftover proteins, LFQ values were normalized by median centering within conditions (normalizedD function of the R package DAPAR (Wieczorek, Combes et al., 2017)). Remaining proteins without any LFQ value in one of both conditions have been considered as proteins quantitatively present in a condition and absent in another. They have therefore been set aside and considered as differentially abundant proteins. Next, missing values were imputed using the imp.norm function of the R package norm. Proteins with a foldchange under 2 have been considered not significantly differentially abundant. Statistical testing of the remaining proteins (having a foldchange over 2) was conducted using a limma t-test thanks to the R package limma (Ritchie, Phipson et al., 2015). An adaptive Benjamini-Hochberg procedure was applied on the resulting p-values thanks to the function adjust.p of R package cp4p using the robust method of Pounds and Cheng to estimate the proportion of true null hypotheses among the set of statistical tests (Pounds & Cheng, 2006). The proteins associated to an adjusted p-value inferior to an FDR level of 1% have been considered as significantly differentially abundant proteins.

## **Adhesion assay**

Adhesion assays were performed as described previously (Vromman et al., 2014). In brief, MEFs cells plated in 24-well plate the day before (100 000 cells/well) were pre-cooled 30 min at 4 °C and then were incubated for 4 h at 4 °C with L2<sup>IncD</sup>GFP bacteria at a MOI = 10, sonicated prior to infection in order to disrupt bacterial aggregates. Then cells were washed gently with PBS and detached using 0.5 mM EDTA in PBS. Samples were fixed 30 min in 2 % PFA, washed with PBS and analyzed using flow cytometry.

## **Bacterial entry assessment**

Entry experiments were performed as described previously (Vromman et al., 2014). In brief, MEFs cells plated on coverslips in 24-well plate the day before (100 000 cells/well) were pre-

cooled 30 min at 4 °C and then incubated for 45 min at 4 °C with L2<sup>IncD</sup>GFP bacteria at a MOI = 10, sonicated prior to infection in order to disrupt bacterial aggregates. Then pre-warmed medium was added and coverslips were incubated at 37 °C before being fixed at different time points in 4 % PFA for 20 min. Extracellular bacteria were stained with a mouse anti-MOMP-LPS (Argene # 11-114) antibody followed with Cy5-conjugated anti-mouse (#PA45002, Amersham Biosciences) secondary antibody. The dilutions were made in PBS containing 3 % of BSA. DNA was stained using 0.5 µg.mL<sup>-1</sup> of Hoechst 33342 (Thermo Fisher Scientific) added in the secondary antibody solution. Images were acquired on an Axio observer Z1 microscope equipped with an ApoTomemodule (Zeiss, Germany) and a 63× Apochromat lens. Images were taken with an ORCAflash4.OLT camera (Hamamatsu, Japan) using the software Zen.

### Progeny assay

For glucose privation tests on MEFs cells, 140 000 cells per well were seeded in a glucose-free DMEM (Invitrogen) supplemented with 10 % FBS. The following day, the medium was replaced with glucose-free DMEM supplemented with 10 % FBS and the indicated concentration of glucose (Sigma). The next day cells were infected with L2<sup>IncD</sup>GFP bacteria at a MOI = 0.2. For progeny assays on HeLa cells, primary cells or MEFs cells, 100 000 cells were seeded in a 24-well plate. The next day cells were pre-treated with CP4d (or DMSO) or cysteamine (Sigma #30078) (or water) for 2 h and infected with L2<sup>IncD</sup>GFP bacteria at a MOI = 0.15. Cells treated with siRNA for 48 h were directly infected with L2<sup>IncD</sup>GFP bacteria or *C. muridarum* at a MOI = 0.2. Thirty hpi, cells were detached and fixed in 2 % PFA in PBS prior to flow cytometry analysis in order to evaluate the first round of infection. In duplicate wells, cells were detached, lysed using glass beads and the supernatant was used to infect new untreated cells (or WT cells in the case of MEFs) plated the day before (100 000 cells/well in a 24-well plate), in serial dilution. The next day, 3 wells per condition with an infection lower than 30 % (checked by microscopy) were detached and fixed as described above, before analysis by flow cytometry and determination of the bacterial titer. In the case of *C. muridarum* infections, bacteria were stained after fixation with a rabbit anti-CmGroEL antibody followed with AlexaFluor488-conjugated anti-rabbit secondary antibody (A11034, Invitrogen). Dilutions were made in PBS containing 0.1 % of BSA and 0.05 % of saponin (Sigma). The anti-CmGroEL antibody was obtained by AgroBio (La Ferté Saint-Aubain) by immunizing one New Zeland white rabbit with *C. muridarum* GroEL prepared as described in (Illingworth, Ramsey et al., 2011). Acquisition was performed using a CytoFLEX S (Beckman Coulter) and 50 000 events per sample were acquired and then analyzed using FlowJo (version 10.0.7).

### Infection in mice

Female TG2<sup>-/-</sup> and TG2<sup>+/+</sup> KO mice were kindly provided by Dr. C. Papista (INSERM UMR970, Centre de Recherche Cardiovasculaire, Paris) and maintained in the animal facility of the Institut Pasteur, Paris. All animals are treated with 2.5 mg of medroxyprogesterone (Depo-provera-SC®, Pfizer) 7 days prior to infection to synchronize the menstrual cycle. Mice were intravaginally inoculated with *C. muridarum*, 10<sup>5</sup> IFU per animal. Twenty-five days after infection, animals were sacrificed and the organs excised including cervix, uterine horn and oviduct. The bacterial burden in the excised organs, in the right part of the upper genital tract was measured by qPCR after DNA extraction using the DNeasy Blood and Tissue Kit (Qiagen). The left part of the upper genital tract was excised and rinsed into PBS for the morphological

observation. Hydrosalpinx score was determined as described (Peng, Lu et al., 2011). Procedures involving mice were previously approved by local Animal Ethics Committees and registered with the French authorities (APAFIS#8635-2017012314265571).

#### **RT-qPCR and qPCR**

One hundred twenty-five thousand cells in a 24-well plate were infected or not with *C. trachomatis* serovar LGV L2 at a MOI = 1. Cells were treated with anti-IL-6 receptor antibody (Roactemra®, Roche) CP4d (40 µM) or DMSO 2 hpi, or doxycycline (62.5 ng.mL<sup>-1</sup>, Sigma) 24 hpi. Cells pre-treated with siRNA for 48 h were directly infected with L2<sup>IncD</sup>GFP bacteria at a MOI = 1. For testing the response of HeLa cells to IL-6 treatment, 125 000 cells in 24-well plate were treated with recombinant human IL-6 (R&D Biosystems) for 18hrs.

Total RNAs were isolated 24 or 48 hpi with the RNeasy Mini Kit (Qiagen) with DNase treatment (DNase I, Roche). RNA concentrations were determined with a spectrophotometer NanoDrop (Thermo Fisher Scientific) and normalized to equal contents. Reverse transcription (RT) was performed using the M-MLV Reverse Transcriptase (Promega) and quantitative PCR (qPCR) undertaken on the complementary DNA (cDNA) with LightCycler 480 system using LightCycler 480 SYBR Green Master I (Roche). For the experiments displayed in Fig. S2, a duplicate well was used to extract genomic DNA (gDNA) of each time point using the DNeasy Blood and Tissue Kit (Qiagen). Data were analyzed using the  $\Delta\Delta C_t$  method with the *actin* gene as a control gene (Schmittgen & Livak, 2008). Each RT-qPCR experiment was performed in duplicate and repeated at least three times.

#### **GFPT activity assay**

HeLa cells treated with ionomycin (4 µM) or DMSO for 6 h were detached in lysis buffer containing 0.05 M Tris, 0.15 M NaCl, 5 % glycerol, 0.5% NP-40, protease inhibitor cocktail EDTA-free (Roche), pH 7.5. After lysis at 4 °C, NP-40 concentration was reduced by addition of an excess of reaction buffer (0.05 M Tris, 0.15 M NaCl, 5 % glycerol, protease inhibitor cocktail EDTA-free, pH 7.5) and cell debris were eliminated by centrifugation. Cell lysates were incubated 45 min at 37 °C with 0.6 mg.mL<sup>-1</sup> fructose-6-phosphate (Sigma) and 0.6 mg.mL<sup>-1</sup> glutamine (Sigma). The reaction was stopped by incubating the samples for 5 min at 100 °C and precipitates were removed by centrifugation. Analysis of the samples was performed by high performance anion exchange chromatography (HPAEC, Dionex, model ISC3000) on a CarboPAC-PA1 column (3.2 × 250 mm, Dionex) using 100 mM NaOH, and 720 mM NaOAc in 100 mM NaOH, as eluent A and B, respectively. The column was pre-equilibrated for 20 min in 98 % A + 2 % B. Following sample injection, a gradient run (flow rate 1 mL.min<sup>-1</sup>) was performed as follows: 0–2 min, isocratic step (98 % A + 2 % B), 2–15 min 98 % A + 2 % B – 80 % A + 20 % B, 15–20 min 80 % A + 20 % B – 57 % A + 43 % B, 20–22 min 57 % A + 43 % B – 100 % B, and 22–25 min 100 % B. Samples were detected on a pulsed electrochemical detector.

#### **Bacterial size measurement**

HeLa cells in a 6-well plate, treated with siRNA as described above, were infected every two hours with L2<sup>IncD</sup>GFP bacteria at a MOI = 0.3. The next day, all wells were detached and fixed simultaneously in 2 % PFA and 2.5 % glutaraldehyde (Sigma) in PBS. After 25 min, cells were broken using glass beads, vortexed and syringed (3 times, using 1 mL 26GA x 3/8-inch syringes). Samples were then analyzed by flow cytometry. An exponential culture of *E. coli*,

purified *C. trachomatis* elementary bodies (i.e. the infectious non-replicative form of the bacterium) and non-infected cells prepared the same way were used to gate successively for particles of equal size or smaller than *E. coli* (thereby excluding non-broken cells), larger than elementary bodies (thereby excluding non-dividing bacteria), and with positive green fluorescence (thereby excluding cell debris). The forward-scattered light (FSC-A) was used to compare bacterial diameters. Each data point represents the mean of at least 400 gated events.

## Electron microscopy

One million five hundred thousand cells were transfected with siRNA and infected two days later. Cells were fixed 30 hpi with 2.5 % glutaraldehyde (v/v) (Electron Microscopy Sciences) in 0.1 M cacodylate buffer pH 7.4, for 1 h at room temperature. After several washes in cacodylate they were post-fixed with 1 % osmium tetroxide (w/v) in cacodylate for 1 h. After several washes with water the cells were progressively dehydrated with increasing concentrations of ethanol from 25 % to 100 %. The cells were then gradually embedded in epoxy resin. After overnight polymerization at 60 °C, 50 to 70 nm thin sections were cut in an ultra-microtome (Ultracut, Leica) and cells were imaged after post-staining with uranyl acetate and lead citrate in a T12-FEI transmission EM operated at 120kV.

## DATA AVAILABILITY

The mass spectrometry proteomics data have been deposited to the ProteomeXchange Consortium via the PRIDE partner repository with the dataset identifier PXD017117.

## ACKNOWLEDGEMENTS

We thank Anke Hellberg and Béatrice Niragire for technical assistance, Manuela D'Eletto for TG2<sup>-/-</sup> reconstituted MEFs, Dr Christina Papista for providing mice, Dr Denise Badet-Denisot for the rhGFPT1 plasmid and for advice, Dr Cora Weigert for anti-GFPT antibodies, Vishu Aimanianda Bopaiah for help with HPAEC, Dr Lingling Chen for CmGroEL, Augustin Latourte for Roactemra®. This work was supported by an ERC Starting Grant (NUChLEAR N°282046), the Institut Pasteur (GFP-LIMNEC METINF), the Centre National de la Recherche Scientifique and by GEFLUC. BM was funded by the Ministère de l'Éducation Nationale, de la Recherche et de la Technologie and by Cancéropole Ile-de-France.

## AUTHOR CONTRIBUTIONS

AS, BM, ML and JWK conceived the study and designed the methodology. BM, ML, ST, SP conducted the experiments and performed data analysis and interpretation. YW conducted the experiments with mice and performed data analysis. MD and MM collected and analyzed the mass spectrometry data. RHL and CG collected and analyzed the HGSOC cohort data. JR collected and analyzed the infection data using cells isolated from the fallopian tube. JWK synthesized TG2 inhibitors. AS and BM wrote the original draft of the manuscript. MM, JWK edited the manuscript. AS and BM revised the manuscript. All authors commented on the manuscript. AS supervised the study and secured funding.

CONFLICT OF INTEREST

The authors declare that they have no conflict of interest.

REFERENCES

AbdelRahman YM, Belland RJ (2005) The chlamydial developmental cycle. *FEMS Microbiol Rev* 29: 949-959

Altuntas S, Rossin F, Marsella C, D'Eleto M, Diaz-Hidalgo L, Farrace MG, Campanella M, Antonioli M, Fimia GM, Piacentini M (2015) The transglutaminase type 2 and pyruvate kinase isoenzyme M2 interplay in autophagy regulation. *Oncotarget* 6: 44941-44954

Assrir N, Richez C, Durand P, Guittet E, Badet B, Lescop E, Badet-Denisot MA (2014) Mapping the UDP-N-acetylglucosamine regulatory site of human glucosamine-6P synthase by saturation-transfer difference NMR and site-directed mutagenesis. *Biochimie* 97: 39-48

Brunham RC, Rey-Ladino J (2005) Immunology of Chlamydia infection: Implications for a Chlamydia trachomatis vaccine. *Nature Reviews Immunology* 5: 149-161

Caron NS, Munsie LN, Keillor JW, Truant R (2012) Using FLIM-FRET to Measure Conformational Changes of Transglutaminase Type 2 in Live Cells. *PLoS ONE* 7: e44159-7

Chang Q, Su K, Baker JR, Yang X, Paterson AJ, Kudlow JE (2000) Phosphorylation of human glutamine:fructose-6-phosphate amidotransferase by cAMP-dependent protein kinase at serine 205 blocks the enzyme activity. *J Biol Chem* 275: 21981-7

Cox J, Hein MY, Luber CA, Paron I, Nagaraj N, Mann M (2014) Accurate proteome-wide label-free quantification by delayed normalization and maximal peptide ratio extraction, termed MaxLFQ. *Molecular & cellular proteomics : MCP* 13: 2513-26

D'Eleto M, Farrace MG, Falasca L, Reali V, Oliverio S, Melino G, Griffin M, Fimia GM, Piacentini M (2009) Transglutaminase 2 is involved in autophagosome maturation. *Autophagy* 5: 1145-54

Derré I, Swiss R, Agaisse H (2011) The lipid transfer protein CERT interacts with the Chlamydia inclusion protein IncD and participates to ER-Chlamydia inclusion membrane contact sites. *PLoS Pathog* 7: e1002092

Di Sabatino A, Vanoli A, Giuffrida P, Luinetti O, Solcia E, Corazza GR (2012) The function of tissue transglutaminase in celiac disease. *Autoimmun Rev* 11: 746-53

Eckert RL, Kaartinen MT, Nurminskaya M, Belkin AM, Colak G, Johnson GVW, Mehta K (2014) Transglutaminase Regulation of Cell Function. *Physiol Rev* 94: 383-417

Elwell CA, Ceesay A, Kim JH, Kalman D, Engel JN (2008) RNA interference screen identifies Abl kinase and PDGFR signaling in *Chlamydia trachomatis* entry. *PLoS Pathog* 4: e1000021

871 Farrelly LA, Thompson RE, Zhao S, Lepack AE, Lyu Y, Bhanu NV, Zhang B, Loh Y-HE,  
872 Ramakrishnan A, Vadodaria KC, Heard KJ, Erikson G, Nakadai T, Bastle RM, Lukasak BJ, Zebroski  
873 H, Alenina N, Bader M, Berton O, Roeder RG et al. (2019) Histone serotonylation is a  
874 permissive modification that enhances TFIID binding to H3K4me3. *Nature* 567: 535-539

875 Filiano AJ, Bailey CD, Tucholski J, Gundemir S, Johnson GV (2008) Transglutaminase 2 protects  
876 against ischemic insult, interacts with HIF1beta, and attenuates HIF1 signaling. *FASEB J* 22:  
877 2662-75

878 Folk JE, Mullooly JP, Cole PW (1967) Mechanism of Action of Guinea Pig Liver  
879 Transglutaminase: II. THE ROLE OF METAL IN ENZYME ACTIVATION. *J Biol Chem* 242: 1838-  
880 1844

881 Ford C, Nans A, Boucrot E, Hayward RD (2018) Chlamydia exploits filopodial capture and a  
882 macropinocytosis-like pathway for host cell entry. *PLoS Pathog* 14: e1007051

883 Gehre L, Gorgette O, Perrinet S, Prevost MC, Ducatez M, Giebel AM, Nelson DE, Ball SG, Subtil  
884 A (2016) Sequestration of host metabolism by an intracellular pathogen. *Elife* 5: e12552

885 George Z, Omosun Y, Azenabor AA, Partin J, Joseph K, Ellerson D, He Q, Eko F, Bandea C,  
886 Svoboda P, Pohl J, Black CM, Igietseme JU (2016) The roles of unfolded protein response  
887 pathways in Chlamydiopathogenesis. *J Infect Dis*: jiw569

888 Guilluy C, Rolli-Derkinderen M, Tharaux P-L, Melino G, Pacaud P, Loirand G (2007)  
889 Transglutaminase-dependent RhoA Activation and Depletion by Serotonin in Vascular Smooth  
890 Muscle Cells. *J Biol Chem* 282: 2918-2928

891 Gundemir S, Colak G, Feola J, Blouin R, Johnson GV (2013) Transglutaminase 2 facilitates or  
892 ameliorates HIF signaling and ischemic cell death depending on its conformation and  
893 localization. *Biochim Biophys Acta* 1833: 1-10

894 Gundemir S, Colak G, Tucholski J, Johnson GV (2012) Transglutaminase 2: a molecular Swiss  
895 army knife. *Biochim Biophys Acta* 1823: 406-19

896 Gundemir S, Monteagudo A, Akbar A, Keillor JW, Johnson GVW (2017) The complex role of  
897 transglutaminase 2 in glioblastoma proliferation. *Neuro-oncology* 19: 208-218

898 Haneji T, Koide SS (1989) Transblot identification of biotin-containing proteins in rat liver. *Anal*  
899 *Biochem* 177: 57-61

900 Hollis RL, Churchman M, Michie CO, Rye T, Knight L, McCavigan A, Perren T, Williams A, G.  
901 MW, Kaplan RS, Jayson GC, Oza A, Harkin DP, Herrington CS, Kennedy R, Gourley C (2019) High  
902 EMSY expression defines a BRCA-like subgroup of high grade serous ovarian carcinoma with  
903 prolonged survival and hypersensitivity to platinum. *Cancer* 125: 2772-2781

904 Huang L, Xu A-M, Liu W (2015) Transglutaminase 2 in cancer. *Am J Cancer Res* 5: 2756-2776

905 Hwang JY, Mangala LS, Fok JY, Lin YG, Merritt WM, Spannuth WA, Nick AM, Fiterman DJ, Vivas-  
906 Mejia PE, Deavers MT, Coleman RL, Lopez-Berestein G, Mehta K, Sood AK (2008) Clinical and

907 Biological Significance of Tissue Transglutaminase in Ovarian Carcinoma. *Cancer Res* 68: 5849-  
908 5858

909 Ientile R, Curro M, Caccamo D (2015) Transglutaminase 2 and neuroinflammation. *Amino*  
910 *Acids* 47: 19-26

911 Iismaa SE, Mearns BM, Lorand L, Graham RM (2009) Transglutaminases and disease: lessons  
912 from genetically engineered mouse models and inherited disorders. *Physiol Rev* 89: 991-1023

913 Illingworth M, Ramsey A, Zheng Z, Chen L (2011) Stimulating the Substrate Folding Activity of  
914 a Single Ring GroEL Variant by Modulating the Cochaperonin GroES. *J Biol Chem* 286: 30401-  
915 30408

916 Jackson SP, Tjian R (1988) O-glycosylation of eukaryotic transcription factors: implications for  
917 mechanisms of transcriptional regulation. *Cell* 55: 125-133

918 Jóźwiak P, Forma E, Bryś M, Krzeslak A (2014) O-GlcNAcylation and Metabolic Reprograming  
919 in Cancer. *Frontiers in endocrinology* 5: 145

920 Keresztessy Z, Csoos E, Harsfalvi J, Csomos K, Gray J, Lightowlers RN, Lakey JH, Balajthy Z, Fesus  
921 L (2006) Phage display selection of efficient glutamine-donor substrate peptides for  
922 transglutaminase 2. *Protein Sci* 15: 2466-80

923 Kreppel LK, Hart GW (1999) Regulation of a Cytosolic and Nuclear O-GlcNAc Transferase: ROLE  
924 OF THE TETRATRICOPEPTIDE REPEATS. *J Biol Chem* 274: 32015-32022

925 Kumar S, Donti TR, Agnihotri N, Mehta K (2014) Transglutaminase 2 reprogramming of glucose  
926 metabolism in mammary epithelial cells via activation of inflammatory signaling pathways. *Int*  
927 *J Cancer* 134: 2798-807

928 Lee JH, Jeong J, Jeong EM, Cho SY, Kang JW, Lim J, Heo J, Kang H, Kim IG, Shin DM (2014)  
929 Endoplasmic reticulum stress activates transglutaminase 2 leading to protein aggregation. *Int*  
930 *J Mol Med* 33: 849-55

931 Lee JK, Enciso GA, Boassa D, Chander CN, Lou TH, Pairawan SS, Guo MC, Wan FYM, Ellisman  
932 MH, Sütterlin C, Tan M (2017) Replication-dependent size reduction precedes differentiation  
933 in Chlamydia trachomatis. *Nature Comm*: 1-9

934 Lee KN, Maxwell MD, Patterson MK, Birckbichler PJ, Conway E (1992) Identification of  
935 transglutaminase substrates in HT29 colon cancer cells: use of 5-(biotinamido)pentylamine as  
936 a transglutaminase-specific probe. *Biochimica et Biophysica Acta (BBA) - Molecular Cell*  
937 *Research* 1136: 12-16

938 Li Y, Roux C, Lazereg S, LeCaer JP, Laprevote O, Badet B, Badet-Denisot MA (2007)  
939 Identification of a novel serine phosphorylation site in human glutamine:fructose-6-  
940 phosphate amidotransferase isoform 1. *Biochemistry (Mosc)* 46: 13163-9

941 Liechti G, Kuru E, Packiam M, Hsu Y-P, Tekkam S, Hall E, Rittichier JT, VanNieuwenhze M, Brun  
942 YV, Maurelli AT (2016) Pathogenic Chlamydia Lack a Classical Sacculus but Synthesize a



943 Narrow, Mid-cell Peptidoglycan Ring, Regulated by MreB, for Cell Division. *PLoS Pathog* 12:  
944 e1005590

945 Liu C, Kellems RE, Xia Y (2017) Inflammation, Autoimmunity, and Hypertension: The Essential  
946 Role of Tissue Transglutaminase. *Am J Hypertens* 30: 756-764

947 Majeed M, Krause KH, Clark RA, Kihlström E, Stendahl O (1999) Localization of intracellular  
948 Ca<sup>2+</sup> stores in HeLa cells during infection with *Chlamydia trachomatis*. *J Cell Sci* 112: 35-44

949 Mehul B, Bawumia S, Hughes RC (1995) Cross-linking of galectin 3, a galactose-binding protein  
950 of mammalian cells, by tissue-type transglutaminase. *FEBS Lett* 360: 160-4

951 Nelea V, Nakano Y, Kaartinen MT (2008) Size distribution and molecular associations of plasma  
952 fibronectin and fibronectin crosslinked by transglutaminase 2. *The protein journal* 27: 223-33

953 Nurminkaya M, Beazley KE, Smith EP, Belkin AM (2014) Transglutaminase 2 promotes PDGF-  
954 mediated activation of PDGFR/Akt1 and beta-catenin signaling in vascular smooth muscle cells  
955 and supports neointima formation. *J Vasc Res* 51: 418-28

956 Ojcius D, Degani H, Mispelter J, Dautry-Varsat A (1998) Enhancement of ATP levels and glucose  
957 metabolism during an infection by *Chlamydia*. *J Biol Chem* 273: 7052-8

958 Olson MG, Widner RE, Jorgenson LM, Lawrence A, Lagundzin D, Woods NT, Ouellette SP, Rucks  
959 EA (2019) Proximity Labeling To Map Host-Pathogen Interactions at the Membrane of a  
960 Bacterium-Containing Vacuole in *Chlamydia trachomatis*-Infected Human Cells. *Infect Immun*  
961 87

962 Orrù S, Caputo I, D'Amato A, Ruoppolo M, Esposito C (2003) Proteomics Identification of Acyl-  
963 acceptor and Acyl-donor Substrates for Transglutaminase in a Human Intestinal Epithelial Cell  
964 Line: IMPLICATIONS FOR CELIAC DISEASE. *J Biol Chem* 278: 31766-31773

965 Palucci I, Matic I, Falasca L, Minerva M, Maulucci G, De Spirito M, Petruccioli E, Goletti D,  
966 Rossin F, Piacentini M, Delogu G (2017) Transglutaminase type 2 plays a key role in the  
967 pathogenesis of *Mycobacterium tuberculosis* infection. *J Intern Med*

968 Peng B, Lu C, Tang L, Yeh IT, He Z, Wu Y, Zhong G (2011) Enhanced upper genital tract  
969 pathologies by blocking Tim-3 and PD-L1 signaling pathways in mice intravaginally infected  
970 with *Chlamydia muridarum*. *BMC infectious diseases* 11: 347

971 Pincus JH, Waelsch H (1968) The specificity of transglutaminase. I. Human hemoglobin as a  
972 substrate for the enzyme. *Arch Biochem Biophys* 126: 34-43

973 Pounds S, Cheng C (2006) Robust estimation of the false discovery rate. *Bioinformatics* 22:  
974 1979-87

975 Rasmussen SJ, Eckmann L, Quayle AJ, Shen L, Zhang Y-X, Anderson DJ, Fierer J, Stephens R,  
976 Kagnoff M (1997) Secretion of proinflammatory cytokines by epithelial cells in response to  
977 *Chlamydia* infection suggests a central role for epithelial cells in chlamydial pathogenesis. *J*  
978 *Clin Invest* 99: 77-87

979 Read T, Brunham R, Shen C, Gill S, Heidelberg J, White O, Hickey E, Peterson J, Utterback T,  
980 Berry K, Bass S, Linher K, Weidman J, Khouri H, Craven B, Bowman C, Dodson R, Gwinn M,  
981 Nelson W, DeBoy R et al. (2000) Genome sequences of *Chlamydia trachomatis* MoPn and  
982 *Chlamydia pneumoniae* AR39. *Nucleic Acids Res* 28: 1397-1406

983 Ritchie ME, Phipson B, Wu D, Hu Y, Law CW, Shi W, Smyth GK (2015) limma powers differential  
984 expression analyses for RNA-sequencing and microarray studies. *Nucleic Acids Res* 43: e47

985 Rossin F, D'Eletto M, Macdonald D, Farrace MG, Piacentini M (2012) TG2 transamidating  
986 activity acts as a reostat controlling the interplay between apoptosis and autophagy. *Amino*  
987 *Acids* 42: 1793-802

988 Roth A, Konig P, van Zandbergen G, Klinger M, Hellwig-Burgel T, Daubener W, Bohlmann MK,  
989 Rupp J (2010) Hypoxia abrogates antichlamydial properties of IFN-gamma in human fallopian  
990 tube cells in vitro and ex vivo. *Proc Natl Acad Sci U S A* 107: 19502-7

991 Rother M, Gonzalez E, Teixeira da Costa AR, Wask L, Gravenstein I, Pardo M, Pietzke M,  
992 Gurumurthy RK, Angermann J, Laudeley R, Glage S, Meyer M, Chumduri C, Kempa S, Dinkel K,  
993 Unger A, Klebl B, Klos A, Meyer TF (2018) Combined Human Genome-wide RNAi and  
994 Metabolite Analyses Identify IMPDH as a Host-Directed Target against *Chlamydia* Infection.  
995 *Cell Host Microbe* 23: 661-671.e8

996 Russell DG, VanderVen BC, Lee W, Abramovitch RB, Kim M-j, Homolka S, Niemann S, Rohde  
997 KH (2010) Mycobacterium tuberculosis Wears What It Eats. *Cell Host & Microbe* 8: 68-76

998 Schmittgen TD, Livak KJ (2008) Analyzing real-time PCR data by the comparative CT method.  
999 *Nature Protocols* 3: 1101-1108

1000 Scidmore MA (2005) Cultivation and laboratory maintenance of *Chlamydia trachomatis*. *Curr*  
1001 *Protocols Microbiol*: 11A1.1-11A1.25

1002 Shao M, Cao L, Shen C, Satpathy M, Chelladurai B, Bigsby RM, Nakshatri H, Matei D (2009)  
1003 Epithelial-to-Mesenchymal Transition and Ovarian Tumor Progression Induced by Tissue  
1004 Transglutaminase. *Cancer Res* 69: 9192-9201

1005 Sharma M, Machuy N, Bohme L, Karunakaran K, Maurer AP, Meyer TF, Rudel T (2011) HIF-  
1006 1alpha is involved in mediating apoptosis resistance to *Chlamydia trachomatis*-infected cells.  
1007 *Cell Microbiol* 13: 1573-85

1008 Shi L, Salamon H, Eugenin EA, Pine R, Cooper A, Gennaro ML (2015) Infection with  
1009 Mycobacterium tuberculosis induces the Warburg effect in mouse lungs. *Scientific reports* 5:  
1010 18176

1011 Sohn J, Chae JB, Lee SY, Kim SY, Kim JG (2010) A novel therapeutic target in inflammatory  
1012 uveitis: transglutaminase 2 inhibitor. *Korean J Ophthalmol* 24: 29-34

1013 Stephens RS, Kalman S, Lammel C, Fan J, Marathe R, Aravind L, Mitchell W, Olinger L, Tatusov  
1014 RL, Zhao Q, Koonin EV, Davis RW (1998) Genome sequence of an obligate intracellular  
1015 pathogen of humans: *Chlamydia trachomatis*. *Science* 282: 754-755

1016 Sugimura Y, Hosono M, Wada F, Yoshimura T, Maki M, Hitomi K (2006) Screening for the  
 1017 preferred substrate sequence of transglutaminase using a phage-displayed peptide library:  
 1018 identification of peptide substrates for TGASE 2 and Factor XIIIa. *J Biol Chem* 281: 17699-706  
  
 1019 Suto N, Ikura K, Sasaki R (1993) Expression induced by interleukin-6 of tissue-type  
 1020 transglutaminase in human hepatoblastoma HepG2 cells. *J Biol Chem* 268: 7469-73  
  
 1021 Tarbet HJ, Dolat L, Smith TJ, Condon BM, O'Brien ET, 3rd, Valdivia RH, Boyce M (2018) Site-  
 1022 specific glycosylation regulates the form and function of the intermediate filament  
 1023 cytoskeleton. *Elife* 7  
  
 1024 Tyanova S, Temu T, Cox J (2016) The MaxQuant computational platform for mass  
 1025 spectrometry-based shotgun proteomics. *Nat Protoc* 11: 2301-2319  
  
 1026 Vromman F, Laverriere M, Perrinet S, Dufour A, Subtil A (2014) Quantitative Monitoring of the  
 1027 *Chlamydia trachomatis* Developmental Cycle Using GFP-Expressing Bacteria, Microscopy and  
 1028 Flow Cytometry. *PLoS One* 9: e99197  
  
 1029 Wang X, Hybiske K, Stephens RS (2017) Orchestration of the mammalian host cell glucose  
 1030 transporter proteins-1 and 3 by Chlamydia contributes to intracellular growth and infectivity.  
 1031 *Pathog Dis* 75  
  
 1032 Wieczorek S, Combes F, Lazar C, Gai Gianetto Q, Gatto L, Dorffer A, Hesse AM, Coute Y, Ferro  
 1033 M, Bruley C, Burger T (2017) DAPAR & ProStaR: software to perform statistical analyses in  
 1034 quantitative discovery proteomics. *Bioinformatics* 33: 135-136  
  
 1035 Yang X, Qian K (2017) Protein O-GlcNAcylation: emerging mechanisms and functions. *Nat Rev*  
 1036 *Mol Cell Biol* 18: 452-465  
  
 1037 Zibrova D, Vandermoere F, Göransson O, Pegg M, Mariño KV, Knierim A, Spengler K, Weigert  
 1038 C, Viollet B, Morrice NA, Sakamoto K, Heller R (2017) GFAT1 phosphorylation by AMPK  
 1039 promotes VEGF-induced angiogenesis. *Biochem J* 474: 983-1001  
 1040  
 1041

## LEGENDS TO THE FIGURES

### Figure 1. **TG2 transamidase activity increases during *C. trachomatis* infection along with its expression.**

A – Whole cell lysates were prepared with HeLa cells infected or not for 48 h with *C. trachomatis* L2 (multiplicity of infection MOI=1) in the presence or not of BP. In the indicated samples CP4d was added 2 h before infection. Cell lysates were run on SDS-PAGE, proteins were transferred to a membrane and BP incorporation was revealed with HRP-conjugated streptavidin. BP incorporation is enhanced in infected samples, and is inhibited by CP4d. The two main bands present in all samples correspond to naturally biotinylated host proteins (Haneji & Koide, 1989). After blotting the membrane was stained with Coomassie blue to control for equal loading.

B – Same as in (A), except that where indicated 250  $\mu$ M doxycycline (doxy, left) or 7  $\mu$ M cycloheximide (CHX, right) were added 24 h or 2 hpi, respectively.

C – Whole cell lysates were prepared with TG2<sup>+/+</sup> and TG2<sup>-/-</sup> MEFs infected or not for 48 h with *C. trachomatis* L2 in the presence or not of BP, and analyzed as in (A).

D –Western blot with anti-TG2 antibodies on total cell lysates infected or not with *C. trachomatis* L2 for the indicated time. The histogram displays the mean  $\pm$  SD of TG2 expression relative to actin from four independent experiments, with the results of the Student's ratio-paired t-test. NI: not infected.

E – Cells were infected with *C. trachomatis* L2 (MOI=1) for 24 or 46 h. Where indicated, 40  $\mu$ M CP4d was added 2 hpi. *tgm2* transcripts were measured by real-time RT-PCR and normalized to *actin* transcripts following the  $\Delta\Delta$ Ct method. The data are presented as relative mRNA levels compared to uninfected cells and shown as the mean  $\pm$  SD. Each experiment was performed in duplicate and repeated at least four times. P-values of Student's ratio-paired t-test <0.05 are shown.

F – Cells were treated for 18 h with the indicated concentration of human recombinant IL-6 before measuring TG2 transcription relative to actin like in (E). The data are presented as relative mRNA levels compared to untreated cells and shown as the mean  $\pm$  SD. Each experiment was performed in duplicate and repeated at least three times. P-values of Student's ratio-paired t-test <0.05 are shown.

F – Cells were left uninfected or infected with *C. trachomatis* L2 in the presence of the indicated concentration of anti-IL-6 receptor antibodies. Forty-eight h later TG2 transcription relative to actin was measured like in (E). The data are presented as relative mRNA levels compared to uninfected/untreated cells and shown as the mean  $\pm$  SD. Each experiment was performed in duplicate and repeated at least three times. P-values of Student's ratio-paired t-test <0.05 are shown.

### Figure 2. **TG2 activity is needed for optimal *C. trachomatis* developmental and enhances hydrosalpinx upon *C. muridarum* infection in mice.**

A – HeLa cells were pre-treated with the indicated concentrations of CP4d (or DMSO alone) for 2 h before being infected with L2<sup>incD</sup>GFP at MOI=0.15. Thirty hours later the cells were disrupted and bacterial titers (IFU=inclusion forming unit) were determined by re-infecting fresh HeLa cells as described in the methods. The mean  $\pm$  SD of three independent experiments are shown. P-values of Student's paired t-test are indicated when <0.05.

B – HeLa cells were transfected with control siRNA or two siRNAs against TG2. Two days later, the efficiency of the silencing was assessed by western blot using anti-TG2 antibodies and anti-

actin antibodies as loading control (bottom). Duplicate wells were infected with L2<sup>incD</sup>GFP and progeny was analyzed as in (A) (top). The mean  $\pm$  SD of four independent experiments are shown. P-values of Student's paired t-test are indicated when  $<0.05$ .

C – Same as in (A) except that *C. trachomatis* serovar L2 (left) or D (right) were grown in primary cells isolated from fallopian tubes. For serovar D, IFU were determined 48 hpi. The mean  $\pm$  SD of four to five independent experiments are shown. P-values of Student's paired t-test are indicated when  $<0.05$ .

D – HeLa cells were pre-treated with the indicated concentrations of CP4d (or DMSO alone) for 2 h before being infected with L2<sup>incD</sup>GFP at MOI=0.15. Thirty hours later the cells were fixed and analyzed by flow cytometry. The percentage of infected cells (left) and the mean fluorescence of the infected population (right)  $\pm$  SD are shown for three independent experiments. P-values of Student's paired t-test are indicated when  $<0.05$ . A representative field for each condition is shown, scale bar = 10  $\mu$ m.

E – Primary epithelial cells isolated from fallopian tubes were pre-treated with the indicated concentrations of CP4d (or DMSO alone) for 2 h before being infected with *C. trachomatis* serovar L2 (left) or D (right). Twenty-four hours later the cells were fixed, bacteria were stained using FITC-labeled anti-Chlamydia-LPS antibodies, and the mean size of the inclusions manually determined using ImageJ, on twenty inclusions per experiment. The mean  $\pm$  SD of three independent experiments are shown. P-values of Student's paired t-test are indicated when  $<0.05$ .

F – Mice were infected intravaginally with  $10^5$  IFU of *C. muridarum*. Twenty-five days later the mice were sacrificed and the upper genital tract, from the uterine horn to the oviduct, was collected. The right part was used for bacterial burden assessment (top left). The left part was rinsed with PBS and observed with a binocular magnifier (right) to determine the hydrosalpinx score (bottom left). Each dot represents one mouse, the mean  $\pm$  SD is shown. P-values of Mann-Whitney test are indicated when  $<0.05$ .

### Figure 3. **TG2 controls glucose import.**

A – MEFs were grown for 24 h culture medium complemented with the indicated concentration of glucose before being infected with L2<sup>incD</sup>GFP bacteria (MOI = 0.2). Cells were disrupted 30 h later and the bacterial titer determined by re-infecting fresh wild type cells. The mean  $\pm$  SD of three independent experiments are shown.

B – Cells were infected with *C. trachomatis* L2 (MOI=1) for 24 or 48 h. Where indicated 40  $\mu$ M CP4d was added 2 hpi. *GLUT-1* and *GLUT-3* transcripts were measured by real-time RT-PCR and normalized to *actin* transcripts following the  $\Delta\Delta$ Ct method. The data are presented as relative mRNA levels compared to uninfected cells and shown as the mean  $\pm$  SD. Each experiment was performed in duplicate and repeated four times. P-values of Student's ratio-paired t-test are indicated when  $<0.05$ .

C —Relationship between *TGM2* and *GLUT-1* (top) and *GLUT-3* (bottom) expression across 265 HGSOs. Expression comparisons were performed using Spearman's rank correlation test.

D —HeLa cells were infected with *C. trachomatis* L2 (MOI=1) for 24 or 46 h. *HIF-1 $\alpha$*  transcripts were measured by real-time RT-PCR and normalized to *actin* transcripts. The data are presented as relative mRNA levels compared to uninfected cells and shown as the mean  $\pm$  SD. Each experiment was performed in duplicate and repeated three times. P-values of Student's ratio-paired t-test are  $> 0.05$ .

E — HeLa cells were transfected with control siRNA or two siRNAs against HIF-1 $\alpha$ . Two days later, cells were infected with *C. trachomatis* L2 (MOI=1) for 48 h. The indicated transcripts were measured by real-time RT-PCR and normalized to *actin* transcripts. The data are presented as relative mRNA levels compared to uninfected cells and shown as the mean  $\pm$  SD. Each experiment was performed in duplicate and repeated three times. P-values of Student's ratio-paired t-test are indicated when <0.05.

F — TG2<sup>-/-</sup> MEFs stably transformed or not with the indicated TG2 construct were infected for two days with *C. trachomatis* L2 (MOI=1). Mouse *GLUT-1* transcripts were measured by real-time RT-PCR and normalized to mouse *actin* transcripts. The data are presented as relative mRNA levels compared to uninfected cells and shown as the mean  $\pm$  SD. Each experiment was performed in duplicate and repeated three times. P-values of Student's ratio-paired t-test are indicated when <0.05.

**Figure 4. GFPT is a substrate of TG2 transamidase activity.**

A — HeLa cells were infected with *C. trachomatis* (MOI = 1) and 40  $\mu$ M CP4d was added or not 2 hpi. After 24 h 0.5 mM BP was added and cells were lysed at 48 hpi. Lysates were precipitated with streptavidin-coated beads. After separation with SDS-PAGE, proteins were transferred to a membrane and blotted with anti-GFPT antibody followed with HRP-conjugated secondary antibody.

B — *In vitro* assay testing the ability of purified TG2 to crosslink purified rhGFPT1 with BP. Samples were incubated for 3 h at 37°C before separation by SDS-PAGE. Proteins were transferred to a membrane and BP was revealed using HRP-conjugated streptavidin. rhGFPT1 is 77.5 kDa.

C — GFPT1 sequence: glutamine residues identified by mass spectrometry as cross-linked to BP are in bold letter .

D — *In vitro* assay was performed as described in B using wild type rhGFPT1 (WT), rhGFPT1 Q58N, rhGFPT1 Q328N or rhGFPT1 Q555N as substrates. The reaction was performed at 37 °C for 30 min. After probing with HRP-Streptavidin the membrane was washed and probed with anti-GFPT antibodies followed with HRP-conjugated secondary antibodies. The ratio of modified protein (streptavidin signal) to the total GFPT is shown, normalized to its value with WT rhGFPT1. The mean  $\pm$  SD of five independent experiments is shown, the p-value of the Student's ratio-paired t-test is indicated when <0.05.

E — Lysates of cells treated or not for 6 h with ionomycin were incubated at 37 °C for 45 min with fructose-6-P and glutamine. The production of glucosamine-6-P was measured using HPAEC-PAD. Results of three independent experiments are shown, with mean  $\pm$  SD, and p-value of the Student's paired t-test is indicated (\*P < 0.05).

**Figure 5. TG2 activation results in increased UDP-GlcNAc production.**

A — Schematic view of the hexosamine biosynthesis pathway. Production of glucosamine-6-P by GFPT is the first and rate-limiting step of the pathway that produces UDP-GlcNAc. HK: hexokinase; G6PI: glucose-6-P isomerase; GFPT: glutamine:fructose-6-P amidotransferase; GNA: glucosamine-6-P N-acetyltransferase; PGM3: phosphoglucomutase 3; UAP: UDP-N-acetylglucosamine pyrophosphorylase; OGT: O-GlcNAc transferase OGA: O-GlcNAcase; GlcNAc: N-acetylglucosamine.

B – Endocervical epithelial cells were pre-treated or not with 40  $\mu$ M CP4d for 2 h before addition of the indicated concentration of ionomycin (or an equivalent volume of DMSO) and 0.5  $\mu$ M BP. Six hours later whole cell lysates were analyzed by western blot. The membrane was first blotted with HRP-conjugated streptavidin to detect TG2 activity, then extensively washed and probed with anti-O-GlcNAcylation antibody followed with HRP-conjugated secondary antibodies. Last the membrane was probed with anti-actin as a loading control.

C – The same experimental procedure as described in (B) was applied to HeLa cells treated for 48 h prior to ionomycin treatment (8  $\mu$ M) with siRNA control or directed against TG2.

**Figure 6. Optimal bacterial growth requires GFPT and prevents UDP-GlcNAc accumulation.**

A – HeLa cells were infected or not (NI) with *C. trachomatis* (MOI = 1), then lysed 24 or 48 hpi. After separation with SDS-PAGE, proteins were transferred to a membrane, probed with anti-O-GlcNAcylation antibody followed with HRP-conjugated secondary antibodies. After extensive washes the membrane was blotted again with anti-GFPT and anti-actin antibodies before revelation with HRP-conjugated secondary antibodies.

B – HeLa cells were infected or not with *C. trachomatis* (MOI = 1). Twenty-four hours later, 8  $\mu$ M ionomycin (or DMSO alone) and 0.5 mM BP were added. After 6 h of treatment, cells were lysed and proteins revealed as in (A).

C – HeLa cells treated for 72 h with siRNA targeting GFPT1 or GFPT2 were lysed. After separation with SDS-PAGE, proteins were transferred to a membrane, probed with anti-GFPT and anti-actin antibody before revelation with HRP-conjugated secondary antibodies.

D – HeLa cells were transfected with control siRNA or siRNAs against GFPT or TG2. Two days later the cells were infected for the indicated times (MOI=0.3) before fixation, rupture of the cells and measurement of bacterial diameter. The mean diameter  $\pm$  SD and p-values of Student's paired t-test on 4 independent experiments are shown.

E – HeLa cells treated for 48 h with siRNA targeting GFPT1 or not (siCTRL) were infected with *C. trachomatis* (MOI = 0.15). Thirty hours later cells were fixed and analyzed by flow cytometry. The percentage of infected cells (top) and the mean fluorescence of the infected population (middle)  $\pm$  SD are shown for at least four independent experiments. Duplicate wells were lysed and used to re-infect fresh HeLa cells to determine the bacterial titer (bottom). P-values of Student's ratio-paired t-test are indicated.

F – Schematic view of the outcome of TG2 activation in infection. The increase in TG2 expression and activity in cells infected with *C. trachomatis* results in the up-regulation of the expression of glucose transporters. Increasing quantities of glucose are thus imported in the host cytoplasm and redirected to the vacuole, where they fuel bacterial growth. Parallel to this transcriptional outcome, the transamidating activity of TG2 targets the host enzyme GFPT, thereby boosting the hexosamine biosynthesis pathway. The bacteria consume the resulting UDP-GlcNAc, or an intermediate along this pathway, in particular to sustain bacterial division.

**Expanded View Figure Legends**

**Figure EV1. TG2 is beneficial for bacterial development (related to Figure 2).**

A – HeLa cells were pre-treated with the indicated concentrations of Cysteamine for 2 h before being infected with L2<sup>incD</sup>GFP at MOI=0.15. Thirty hours later the cells were disrupted and bacterial titers (IFU) were determined by re-infecting fresh HeLa cells as described in the

methods. The mean  $\pm$  SD of three independent experiments are shown. P-values of Student's paired t-test are indicated when  $<0.05$ .

B – TG2<sup>+/+</sup> and TG2<sup>-/-</sup> MEFs were infected with L2<sup>incD</sup>GFP at MOI=0.15. Thirty h later the cells were disrupted and bacterial titers were determined by re-infecting fresh TG2<sup>+/+</sup> cells as described in the methods. The mean  $\pm$  SD of five independent experiments and p-values from Student's paired t-test are shown.

C – To measure bacterial adhesion TG2<sup>+/+</sup> and TG2<sup>-/-</sup> MEFs were incubated at 4 °C for 4 h with L2<sup>incD</sup>GFP at MOI=10 before being washed and fixed as described in the methods. The mean  $\pm$  SD of three independent experiments are shown.

D – TG2<sup>+/+</sup> and TG2<sup>-/-</sup> MEFs were infected with L2<sup>incD</sup>GFP at MOI=10 and fixed at the indicated time. Extracellular bacteria were differentially labeled as described in the methods. The mean  $\pm$  SD of three independent experiments, and p-values from Student's paired t-test, are shown.

**Figure EV2. Infection by *C. muridarum* activates TG2, which favors bacterial growth** (related to Figure 2).

A – Whole cell lysates were prepared with HeLa cells infected or not for 48 h with *C. muridarum* (MOI=1) in the presence or not of BP. Cell lysates were run on SDS-PAGE, proteins were transferred to a membrane and BP incorporation was revealed with HRP-conjugated streptavidin.

B – HeLa cells were transfected with siRNA against TG2 for 48 h before being infected in duplicates with *C. muridarum* at MOI=0.15. Thirty hours later one set of cells were disrupted and bacterial titers (IFU=inclusion forming unit) were determined by re-infecting fresh HeLa cells as described in the methods. The mean  $\pm$  SD of three independent experiments and p-values of Student's paired t-test are shown (top). Duplicate wells were incubated further for a total of 48 h before the cells were fixed, permeabilized with 0.3% Triton-X100 and stained with rabbit antibodies against *C. muridarum* GroEL followed with A488-coupled anti-rabbit secondary antibodies. Samples were analyzed by flow cytometry, the percentage of infected cells (middle) and the mean fluorescence of the infected population (bottom)  $\pm$  SD are shown for three independent experiments, p-values of Student's paired t-test are indicated.

**Figure EV3. GFPT silencing affects bacterial division** (related to Figure 6).

HeLa cells treated for 48 h with siRNA targeting GFPT1 or not (siCTRL) were infected with *C. trachomatis* (MOI = 1), fixed 30 hpi and processed for transmission electron microscopy. Lines show example of measured RB diameters. Scale bar = 600 nm. RB diameters were measured using ImageJ on > 300 bacteria in one experiment. Each dot represents one RB, the mean value  $\pm$  SD and p-value of Student's paired t-test are indicated.



Figure 1

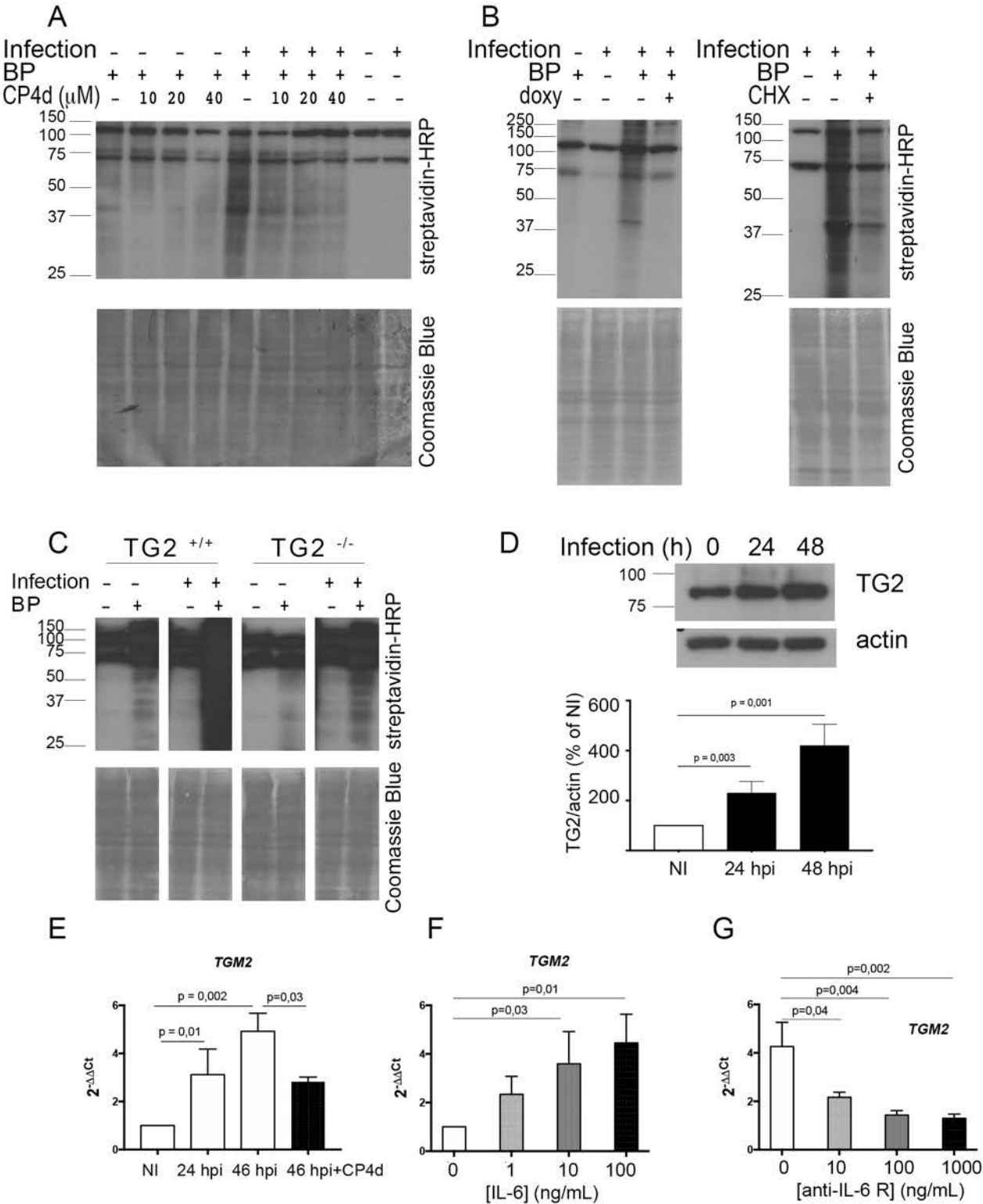


Figure 2

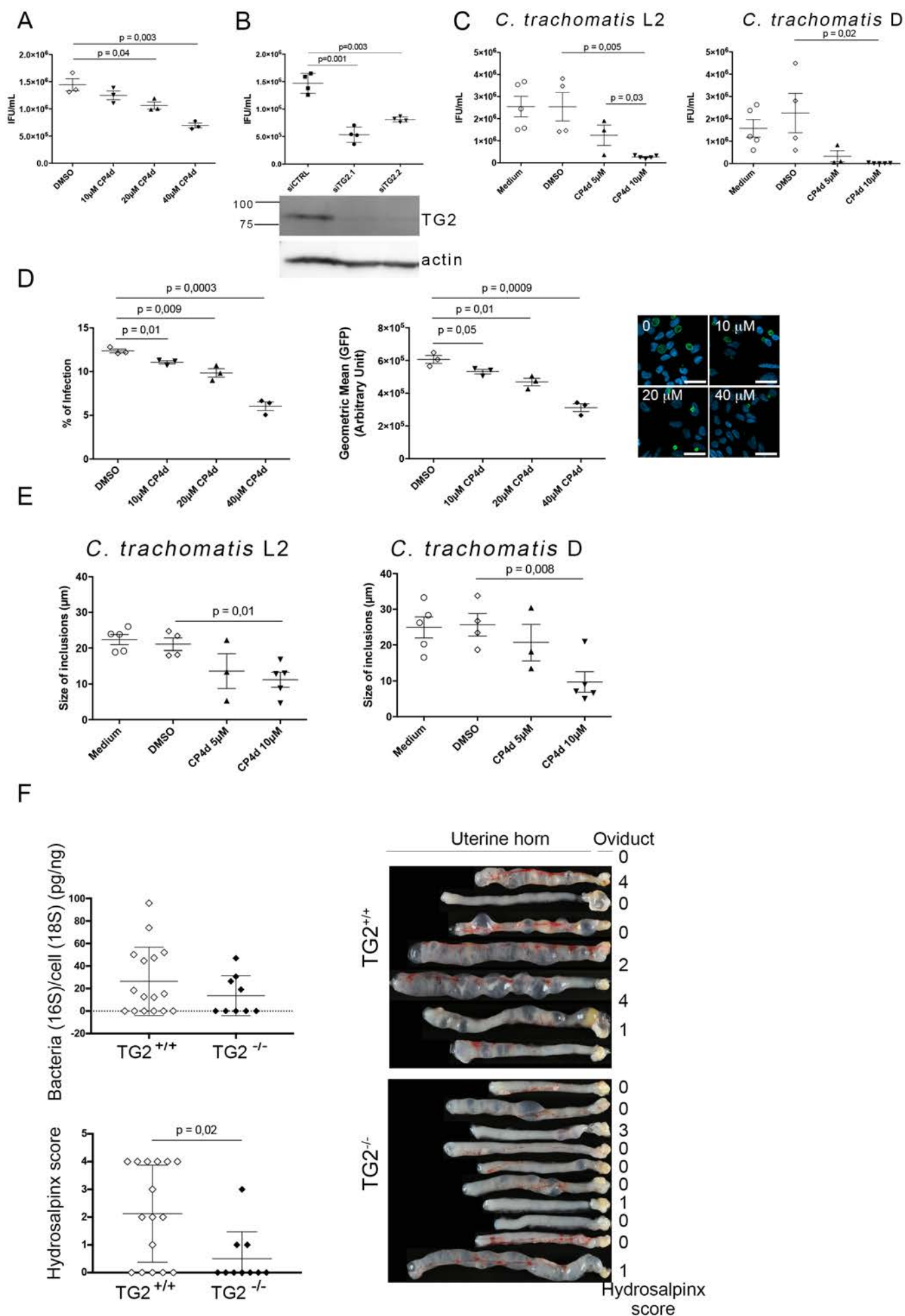


Figure 3

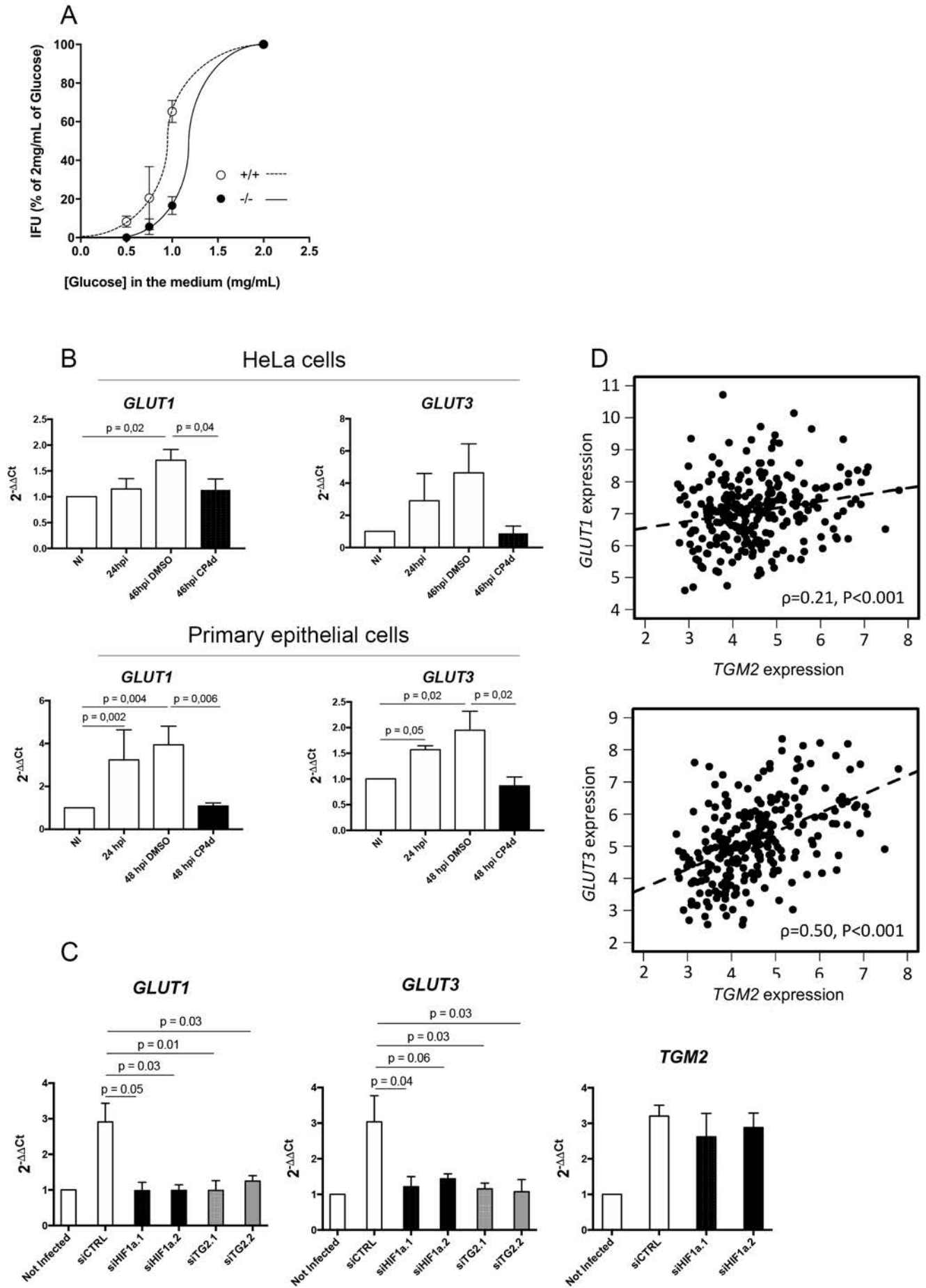


Figure 4

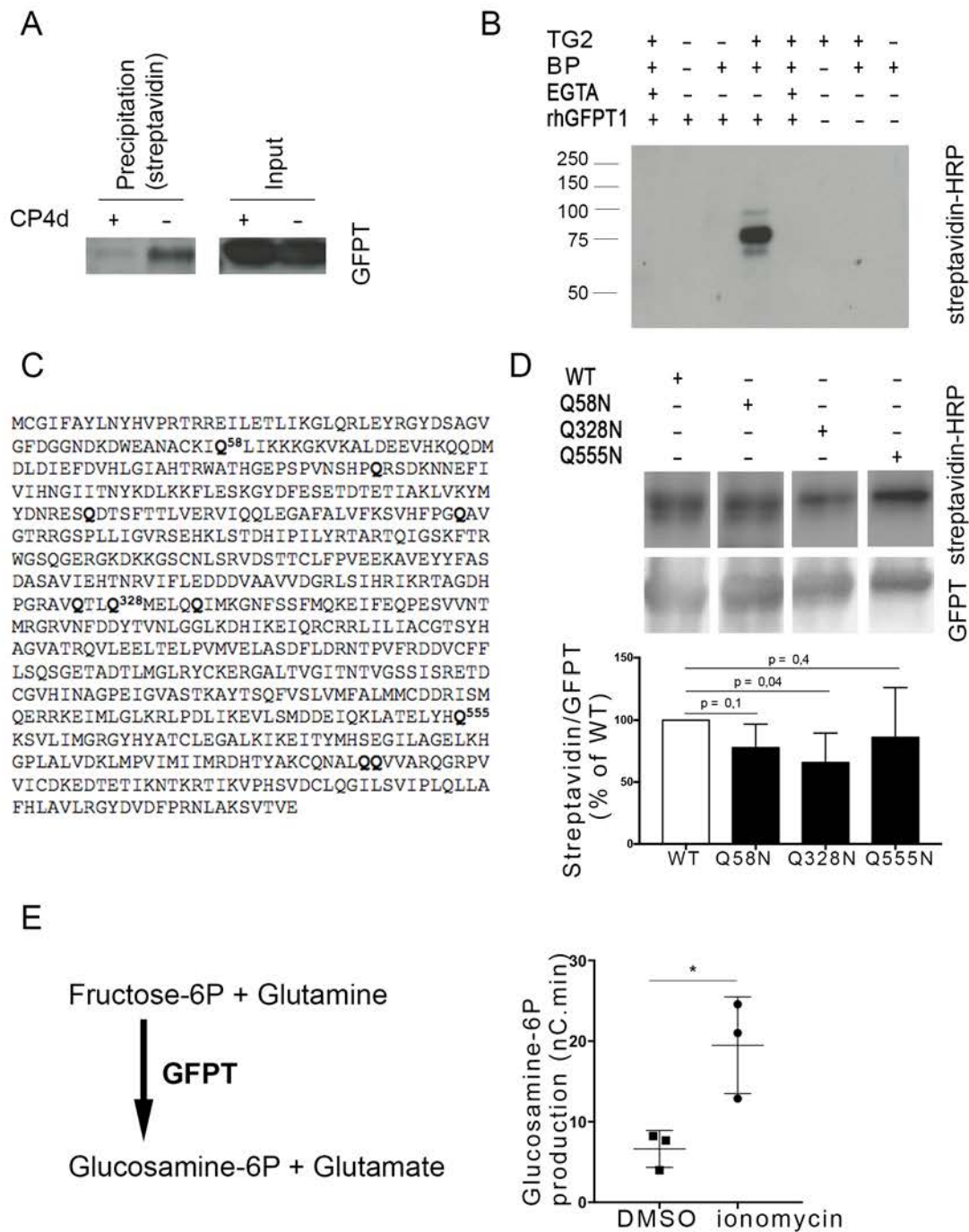


Figure 5

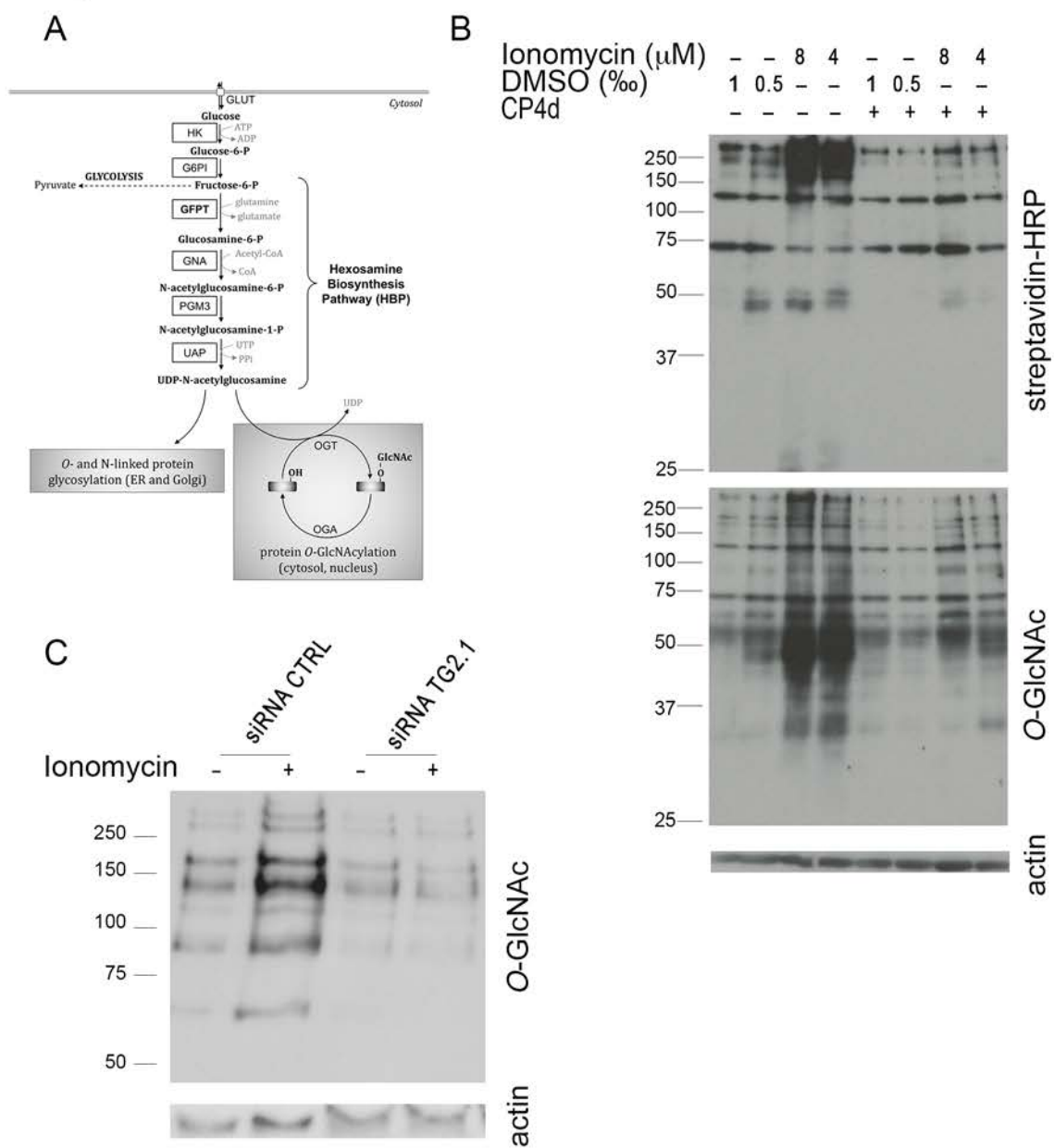


Figure 6

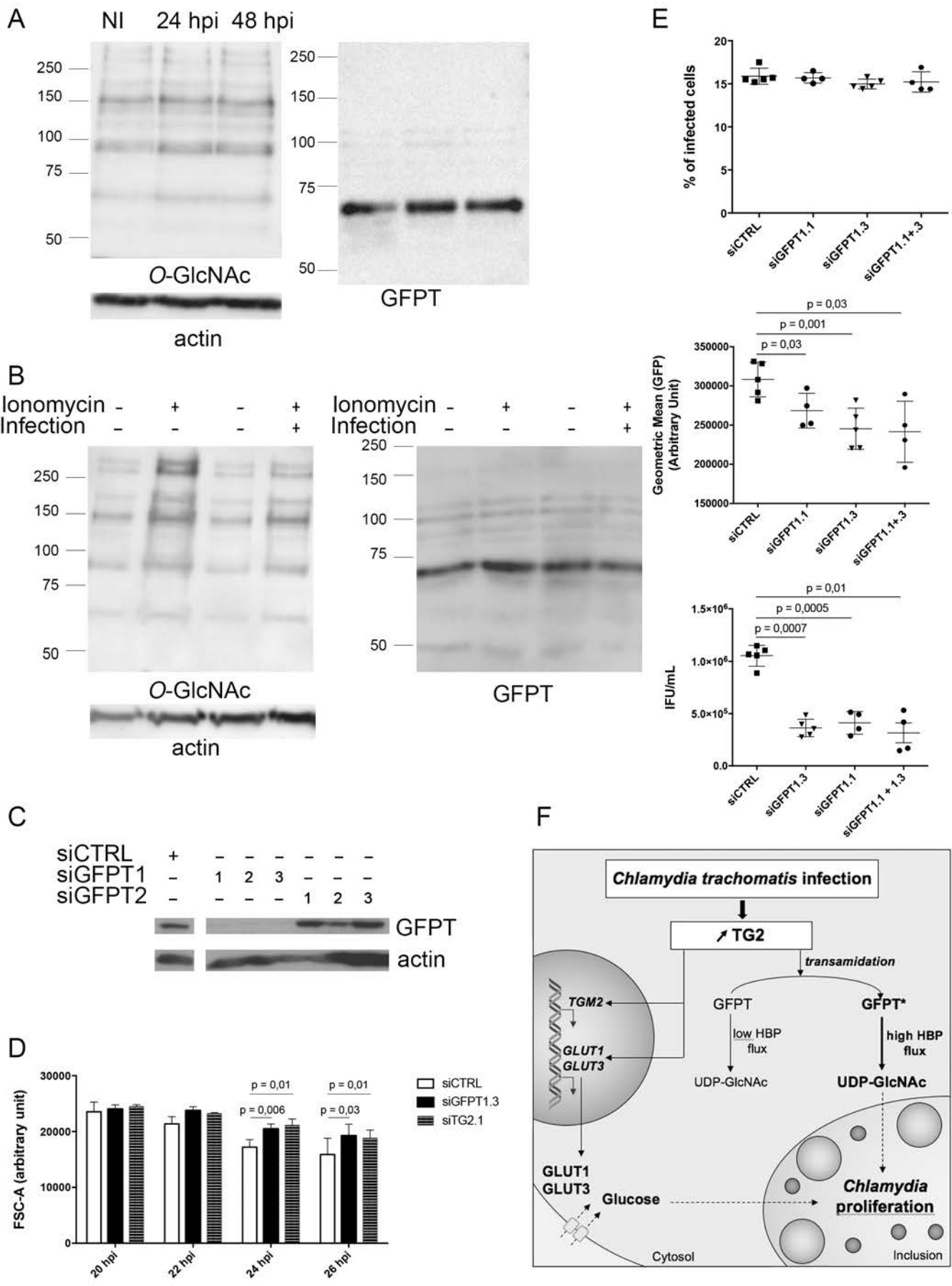
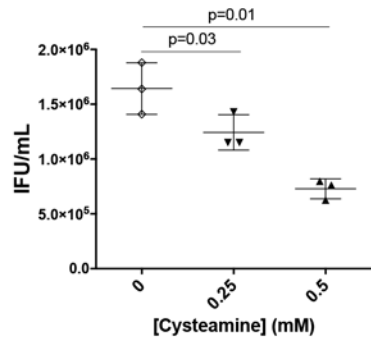
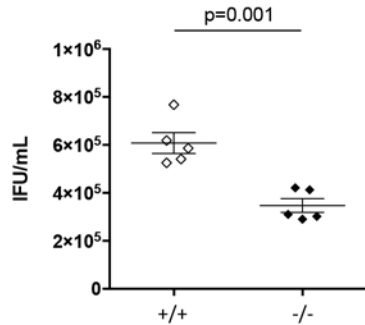


Figure EV1

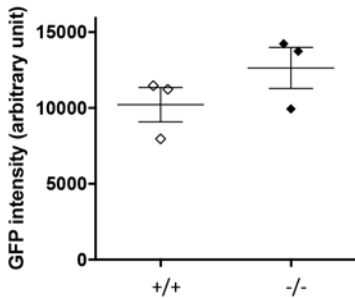
A



B



C



D

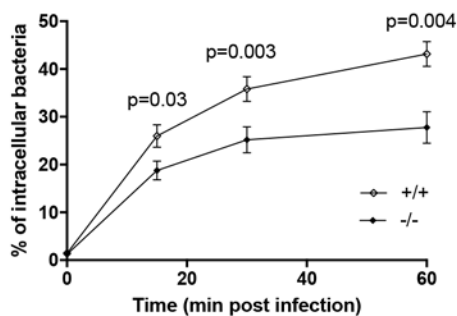
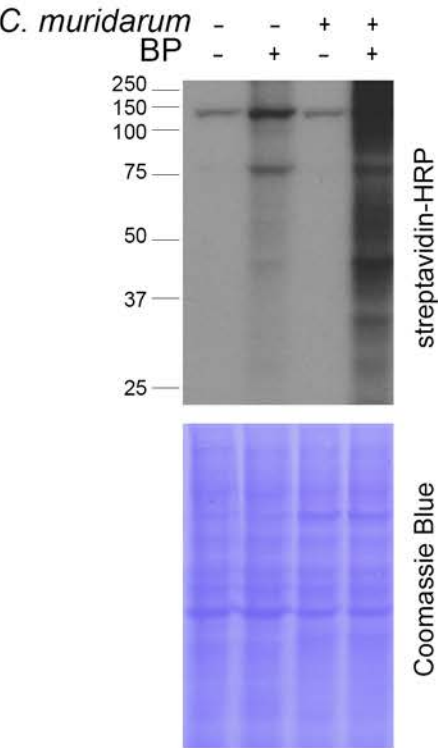


Figure EV2

A



B

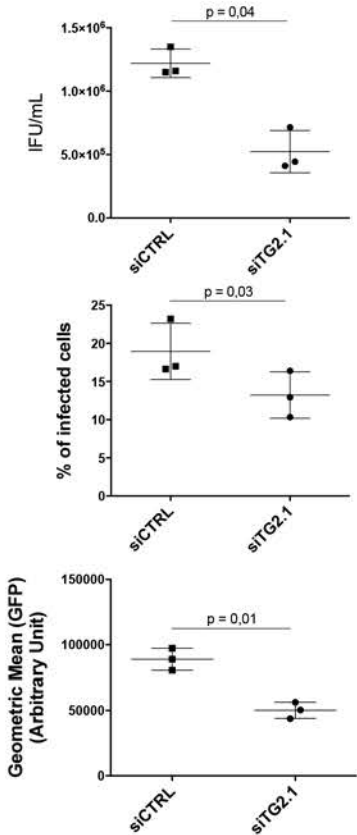
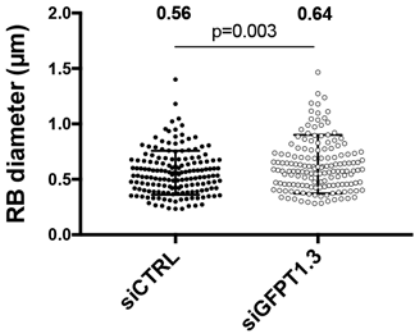
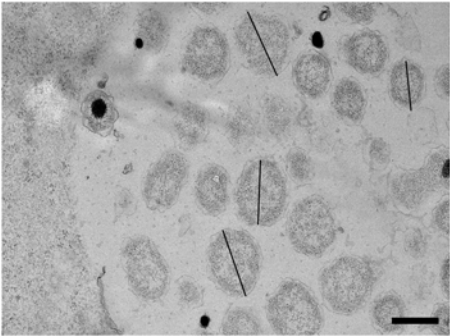




Figure EV3



Infection-driven activation of transglutaminase 2 boosts glucose uptake and hexosamine biosynthesis

Benoit Maffei<sup>1,2</sup>, Marc Laverrière<sup>1</sup>, Yongzheng Wu<sup>1</sup>, Sébastien Triboulet<sup>1</sup>, Stéphanie Perrinet<sup>1</sup>, Magalie Duchateau<sup>3</sup>, Mariette Matondo<sup>3</sup>, Robert L. Hollis<sup>4</sup>, Charlie Gourley<sup>4</sup>, Jan Rupp<sup>5</sup>, Jeffrey W. Keillor<sup>6</sup> and Agathe Subtil<sup>1\*</sup>

APPENDIX

Table of contents:

- Legends to the supplementary figures
- Figure S1. **Live bacteria induce TG2 activation in HeLa and MEFs cells.**
- Figure S2. **Reduction of bacterial load does not account for the loss of induction of *GLUT-1* and *GLUT-3* transcription upon CP4d treatment.**
- Figure S3. **Measure of glucosamine-6-P production by GFPT by HPAEC-PAD.**
- Figure S4. **Gating steps for the examination of the size of replicative *C. trachomatis* by flow cytometry.**
- Table S1. **Candidate TG2 substrates in *C. trachomatis* infected cells**
- Table S2. **Primers used for siRNA, qPCR and mutagenesis**

## Legends

Figure S1. **Live bacteria induce TG2 activation in HeLa and MEFs cells.** Related to Figure 1. Before addition to HeLa cells the bacterial inoculum was either left untreated (MOI = 1), or filtered through of a 0.22  $\mu$ M filter, or incubated for 30 min at 65 °C to kill the bacteria. The inoculum was applied to HeLa cells in the presence or not of BP and 48 h later whole cell lysates were prepared. After separation by SDS-PAGE, proteins were transferred to a membrane and BP incorporation was revealed with HRP-conjugated streptavidin.

Figure S2. **Reduction of bacterial load does not account for the loss of induction of *GLUT-1* and *GLUT-3* transcription upon CP4d treatment.** Related to Figure 3. HeLa cells were infected or not with *C. trachomatis* (MOI=1) in duplicate per condition. Two hpi CP4d (40  $\mu$ M) or 24 hpi doxycycline (62.5 ng.mL<sup>-1</sup>) were added to the culture medium. Forty-eight hpi DNA were extracted from one well to measure bacterial load, and RNA were extracted from the duplicate well. Bacterial gDNA (16S RNA) measured by real-time RT-PCR was normalized to host gDNA (*actin* gene) and is expressed relative to the infected non-treated culture. *GLUT-1* and *GLUT-3* transcripts were measured by real-time RT-PCR and normalized to *actin* with the  $\Delta\Delta$ Ct method as in Fig. 3A. The experiment was performed in duplicate and repeated four times, mean  $\pm$  SD are shown. P-values of the Student's ratio-paired t-test are indicated when <0.05.

Figure S3. **Measure of glucosamine-6-P production by GFPT by HPAEC-PAD.** Related to Figure 4. The three top panels show the retention times of the different sugars used or produced during the reaction when analyzed by HPAEC-PAD. Note that glutamine and glutamate are not retained by this column. A cell lysate without addition of fructose-6-P or glutamine is also shown. The bottom two panels display an enlargement of the output of the reaction when control or ionomycin treated cell lysates were used. The arrows point to the glucosamine-6-P peak. Fructose-6-P was not entirely consumed by the reaction. Formation of glucose-6-P was also observed, possibly by GFPT isomerase activity or by another cellular enzyme present in the lysate such as glucose-6-P isomerase.

Figure S4. **Gating steps for the examination of the size of replicative *C. trachomatis* by flow cytometry.** Related to Figure 6. Exponential cultures of *E. coli*, density-gradient purified elementary bodies, non-infected cells, and cells infected with L2<sup>incD</sup>GFP at MOI=0.3 for different time points (indicated) were fixed and treated as described in the methods section. The top dot plots describe how the first three samples were used to gate the region of interest that contains mostly replicative *C. trachomatis* (excluded regions are hatched). An increase in the number of replicative bacteria, and a decrease in their size (FSC-A value) were observed when increasing infection time.

Figure S1

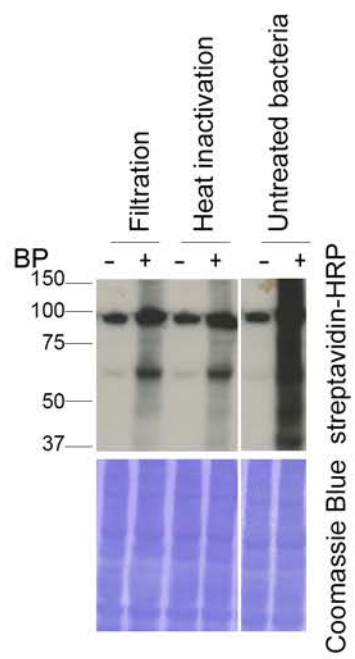


Figure S2

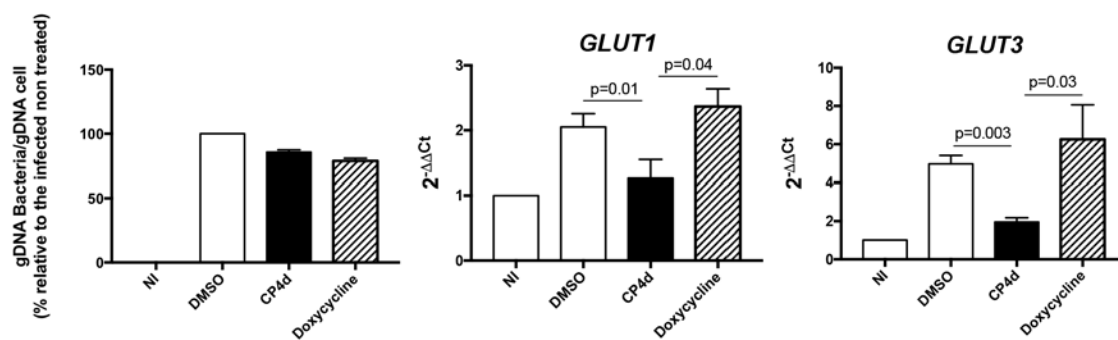
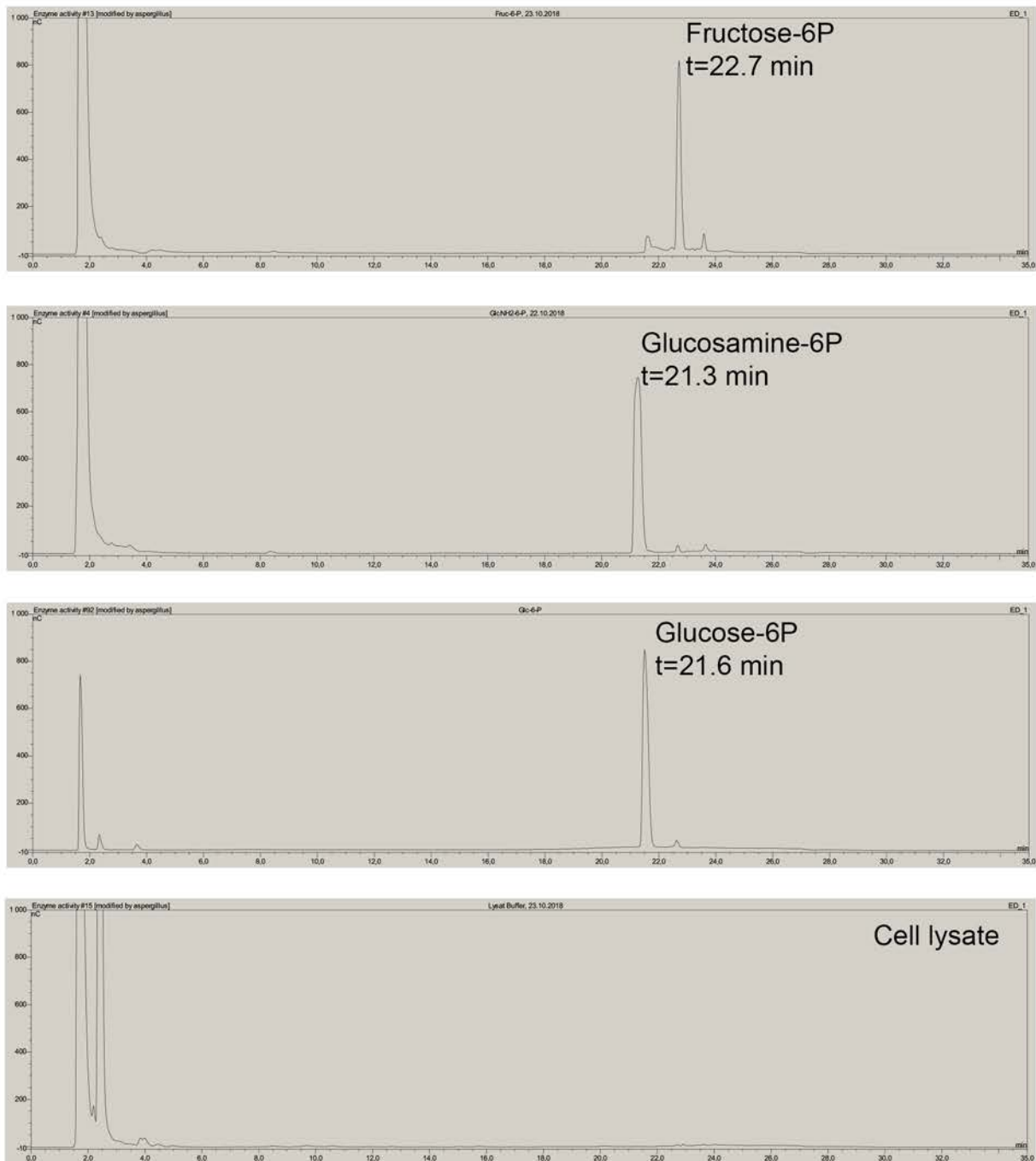


Figure S3



Reaction products:

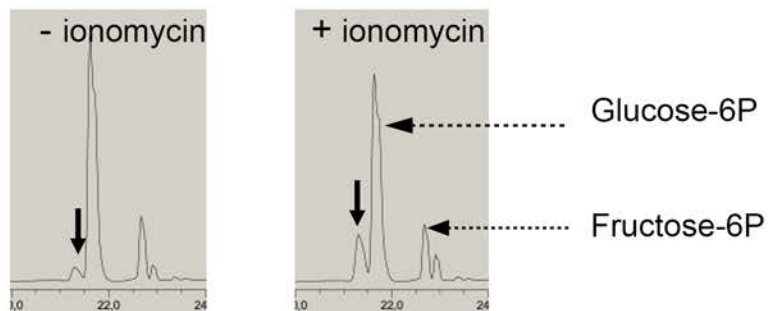
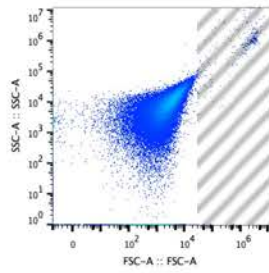
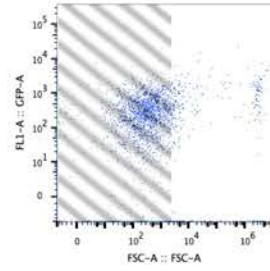


Figure S4

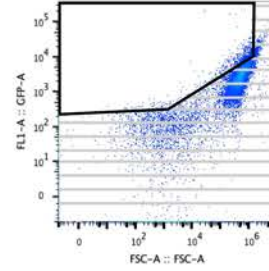
1- Gating on *E. coli*



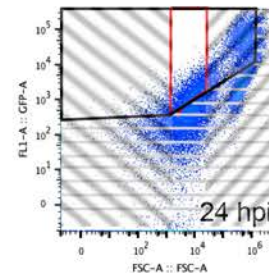
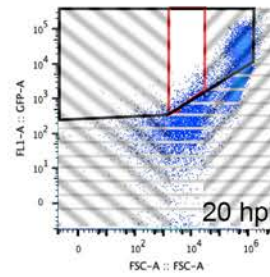
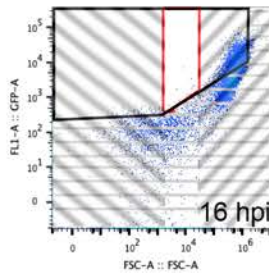
2-Exclusion of non-diving bacteria (elementary bodies)



3- Exclusion of cell debris



4 - Infected samples analysis



Infection time (h)	16	20	24
Number of events gated	53	1300	5596
FSC-A Geometric Mean	24688	18135	14445

**Table S1: Candidate TG2 substrates in *C. trachomatis* infected cells**

The list displays streptavidin-bound proteins identified by mass spectrometry in the infected samples only in the presence of BP (first 37 entries) or more abundant in the presence of BP than in its absence (last 25 entries,  $\text{Log}_2([\text{Mean intensity with BP}]/[\text{Mean intensity without BP}])$  and p-values are shown).

UniProt ID	Protein	Gene	Protein description	log2	P-value
Q8NE71-2	ABCF1	ABCF1	ATP-binding cassette sub-family F member 1	NA	NA
O95831-3	AIFM1	AIFM1	Apoptosis-inducing factor 1	NA	NA
P50995-2	ANX11	ANXA11	Annexin A11	NA	NA
P84077	ARF1	ARF1	ADP-ribosylation factor 1	NA	NA
Q13510	ASAH1	ASAH1	Acid ceramidase	NA	NA
Q12797-10	ASPH	ASPH	Aspartyl/asparaginyl beta-hydroxylase	NA	NA
P36542-2	ATPG	ATP5C1	ATP synthase subunit gamma	NA	NA
O95816	BAG2	BAG2	BAG family molecular chaperone regulator	NA	NA
Q13185	CBX3	CBX3	Chromobox protein homolog 3	NA	NA
Q9Y696	CLIC4	CLIC4	Chloride intracellular channel protein 4	NA	NA
Q16555-2	DPYL2	DPYSL2	Dihydropyrimidinase-related protein	NA	NA
P55884	EIF3B	EIF3B	Eukaryotic translation initiation factor 3 subunit B	NA	NA
P02751-4	FINC	FN1	Fibronectin	NA	NA
G3V1Q4	G3V1Q4	SEPT7	Septin 7	NA	NA
Q9HAV0	GBB4	GNB4	Guanine nucleotide-binding protein subunit beta	NA	NA
O94808	GFPT2	GFPT2	Glutamine--fructose-6-phosphate aminotransferase	NA	NA
P08754	GNAI3	GNAI3	Guanine nucleotide-binding protein G(k) subunit alpha	NA	NA
H3BSW3	H3BSW3	APRT	Adenine phosphoribosyltransferase	NA	NA
P68871	HBB	HBB	Hemoglobin subunit beta	NA	NA



A0A087WZW8	IGKV3-11	IGKV3-11	Ig kappa chain C region	NA	NA
Q15181	IPYR	PPA1	Inorganic pyrophosphatase	NA	NA
J3QLE5	J3QLE5	SNRPN	Small nuclear ribonucleoprotein-associated protein N	NA	NA
K7ENG2	K7ENG2	U2AF2	Splicing factor U2AF 65 kDa subunit	NA	NA
P17931	LEG3	LGALS3	Galectin-3	NA	NA
C9JIG9	OSR1	OSXR1	Serine/threonine-protein kinase OSR1	NA	NA
P17858	PFKAL	PFKL	ATP-dependent 6-phosphofructokinase	NA	NA
E9PQ98	PRMT1	PRMT1	Protein arginine N-methyltransferase 1	NA	NA
P62195-2	PRS8	PSMC5	26S proteasome regulatory subunit 8	NA	NA
O00487	PSDE	PSMD14	26S proteasome non-ATPase regulatory subunit	NA	NA
Q16401-2	PSMD5	PSMD5	26S proteasome non-ATPase regulatory subunit 5	NA	NA
Q06203	PUR1	PPAT	Amidophosphoribosyltransferase	NA	NA
P17812-2	PYRG1	CTPS1	CTP synthase 1	NA	NA
P43487-2	RANG	RANBP1	Ran-specific GTPase-activating protein	NA	NA
Q9P2E9-2	RRBP1	RRBP1	Ribosome-binding protein 1	NA	NA
P56192	SYMC	MARS	Methionine--tRNA ligase	NA	NA
O95497	VNN1	VNN1	Pantetheinase	NA	NA
E9PRD9	VNN2	VNN2	Vascular non-inflammatory molecule 2	NA	NA
P08243-2	ASNS	ASNS	Asparagine synthetase	7,62	1,81E-08
P30508	HLA-C	HLA-C	HLA class I histocompatibility antigen, Cw-12 alpha chain	9,05	4,07E-08
P35613-2	BASI	BSG	Basigin	2,33	1,85E-05
P10909-4	CLUS	CLU	Clusterin	2,13	3,91E-05

P49368	TCPG	CCT3	T-complex protein 1 subunit gamma	1,83	3,99E-04
O15427	MOT4	SLC16A3	Monocarboxylate transporter 4	1,93	6,21E-04
E9PLL6	RPL27A	RPL271	60S ribosomal protein L27a	1,36	9,12E-04
Q15233	NONO	NONO	Non-POU domain-containing octamer-binding protein	1,26	1,21E-03
P30837	AL1B1	ALDH1B1	Aldehyde dehydrogenase X	1,98	1,50E-03
E9PLA9	CAPRIN1	CAPRIN	Caprin-1	1,47	1,61E-03
P17987	TCPA	TCP1	T-complex protein 1 subunit alpha	1,91	2,84E-03
P39019	RS19	RPS19	40S ribosomal protein S19	1,44	3,74E-03
O43143	DHX15	DHX15	Putative pre-mRNA-splicing factor ATP-dependent RNA helicase	1,00	4,00E-03
P61586	RHOA	RHOA	Transforming protein RhoA	1,01	4,49E-03
C9J9K3	RPSA	RPSA	40S ribosomal protein SA	1,07	4,91E-03
A0A087WXM6	RPL17	RPL17	60S ribosomal protein L17	1,01	5,48E-03
P38919	EIF4A3	EIF4A3	Eukaryotic initiation factor 4A-III	1,08	7,23E-03
P00505	AATM	GOT2	Aspartate aminotransferase, mitochondrial	1,11	8,63E-03
P27105	STOM	STOM	Erythrocyte band 7 integral membrane protein	1,01	9,61E-03
A0A096LNZ9	ISG15	ISG15	Ubiquitin-like protein ISG15	1,25	1,10E-02
E9PEX6	DLD	DLD	Dihydrolipoyl dehydrogenase, mitochondrial	1,08	1,66E-02
Q10589-2	BST2	BST2	Bone marrow stromal antigen 2	1,15	2,37E-02
Q06210	GFPT1	GFPT1	Glutamine--fructose-6-phosphate aminotransferase	3,22	2,49E-02
A0A087WVM3	CYR61	CYR61	Protein CYR61	1,34	2,75E-02
Q13162	PRDX4	PRDX4	Peroxisredoxin-4	1,13	2,88E-02

**Table S2: Primer sequences used for siRNA, qPCR and mutagenesis**

Experiment	Target	Sequence
siRNA	TG2.1	GGGCGAACCACCUGAACAAAdTdT
	TG2.2	CAGUUCGAGGAUGGAAUCCUGGAUAdTdT
	HIF1 $\alpha$ .1	AAGUCUGCAACAUGGAAGGUAdTdT
	HIF1 $\alpha$ .2	UUCUCCGAACGUGUCACGUdTdT
	GFPT1.1	GACAGAUUGUGGAGUUCAUdTdT
	GFPT1.2	CCUUGGUGGAGAGAGUUAUdTdT
	GFPT1.3	GUGACUUCUGGACAGAAAdTdT
	GFPT2.1	GUUCCAAGUUUGCGUAUAAAdTdT
	GFPT2.2	GACCGAAUUUCACUACAAAdTdT
	GFPT2.3	CCAUCGCCAAGCUGAUUAAAdTdT
qPCR	$\alpha$ -actin	GGACTTCGAGCAAGAGATGG
		GCAGTGATCTCCTTCTGCATC
	<i>Chlamydia</i> 16S RNA	TGGATGAGGCATGCAAGTA
		TACTAACCCCTCCGCCACTAAA
	Mouse 18S RNA	TAACGAACGAGACTCTGGCAT
		CGGACATCTAAGGGCATCACAG
	TG2	TAAGAGATGCTGTGGAGGAG
		CGAGCCCTGGTAGATAAA
	GLUT-1	AACTCTTCAGCCAGGGTCCAC
		CACAGTGAAGATGATGAAGAC
Mutagenesis	Q58N	GGGAAGCCAATGCCTGCAAAATCAATCTTATTAAGAAGAAAGGAAAAGT
		ACTTTTCCTTCTTCTTAATAAGTTGATTTGCAGGCATTGGCTTCCC
	Q326N	CGAGCTGTGCAAACTCAATATGGAATCCAGCAGATC
		GATCTGCTGGAGTTCATATTGAGTGTTGCACAGCTCG
	Q548N	CGAAATTCAGAACTAGCAACAGAACTTTATCATAATAAGTCAGTTCTGATAATG
		CATTATCAGAACTGACTTATTATGATAAAGTTCTGTTGCTAGTTTCTGAATTCG